Progress in Nuclear Energy 189 (2025) 105940

Contents lists available at ScienceDirect

Progress in Nuclear Energy

journal homepage: www.elsevier.com/locate/pnucene

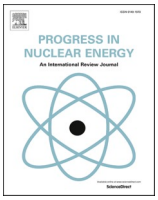

A neutronic model to find promising candidates as burnable poisons in fast reactors

Roberto Pergreffi [a,*], Francesco Lodi [a], Giacomo Grasso [a], Alessia Di Francesco [b]

[a] ENEA – Italian National Agency for New Technologies, Energy and Sustainable Economic Development, Via Dei Mille 21, 40121, Bologna, Italy
[b] Newcleo Srl, Via Galliano 27, 10129, Torino, Italy

ARTICLE INFO

Keywords:
Burnable poisons
Small modular liquid metal fast reactors
Reactivity swing
Transmutation

ABSTRACT

Small modular liquid-metal-cooled fast reactors may require dedicated provisions to reach very long core lifetime, or to reduce the reactivity swing if minimizing control requirements is needed. In such cases, the use of burnable poisons may be a necessary route. Unfortunately, to date very few materials are known that may be used as burnable poisons in fast reactors. Goal of this paper is therefore to propose a model by which the expected neutronic behavior of a candidate burnable poison material in fast spectrum can be estimated without the need for extensive neutronic calculations, for which a detailed description of the system in terms of materials and geometry would be required. The neutronic behavior of a material is estimated by considering separately its performance in terms of poisonousness, defined as the ability to provide enough negative reactivity to compensate for the initial excess reactivity of the fuel, from its performance in terms of burnability, defined as the ability to balance in time the reactivity change due to fuel depletion. Although the values calculated by the model equations do not have physical meaning per se, they can be used to compare different materials with each other in order to make a preliminary assessment of their neutronic behavior. The model was first tested with seven candidates (Eu_2O_3, Gd_2O_3, Dy_2O_3, Er_2O_3, NpO_2, AmO_2 and B_4C), and then assessed against the results obtained from simulations with MCNP6.1 for a lead fast reactor fuel assembly with UO_2 enriched in ^{235}U at 19.75 wt% in which, one at a time, the various candidates have been added. Despite some small differences from the simulations especially at low burnups, the comparison confirmed the prediction capability of the model up to a poison content of 10 at.%.

1. Introduction

Among the many liquid-metal-cooled fast reactor projects currently under development, some are targeting the small reactor range. For these, the small size of the core limits the breeding capability, implying a reactivity swing during operation that can be expected to be relatively large (in particular for those systems that do not consider partial core refueling, in the so called battery approach).

For these systems, the use of burnable poisons (BPs) could be an attractive solution. In fact, as non-fissile materials which compensate for the excess reactivity of the fuel during the early stages of core operational cycles by virtue of their large neutron absorption cross sections [Duderstadt, 1976], the burnable poisons can be used in two alternative ways: either to increase the initial fuel inventory on which the core lifetime depends, and therefore the burnup at discharge, without the penalization of the consequently large excess reactivity, or to reduce the reactivity swing simplifying the reactor control.

Recently, the use of burnable poisons has been explored in a small modular sodium cooled fast reactor (SMSFR) of 128 MWe as a solution to reduce the reactivity swing thus minimizing the effects of control rod withdrawal (CRW) accidents [Guo, 2020]. In particular, two solutions have been investigated: ^{237}Np to 3 wt% homogeneously mixed in all fuel pins, and B_4C with ^{10}B content from 2 to 10 % coupled with Zr_5H_8 in a dedicated control assembly consisting of 20 % absorber and 26 % moderator.

However, despite their strategic importance for small modular fast reactors, to date very few materials are known as viable burnable poisons, mostly because of a rather limited experience with these materials in fast reactors. Indeed, typical (i.e., medium to large) liquid-metal-cooled fast breeder reactors (LMFBRs) have never needed BPs, as they are highly stable and easily controllable [Lamarsh, 2001]. As it is well-known, this is due to the fact that the change in reactivity is much

* Corresponding author.
E-mail address: roberto.pergreffi@enea.it (R. Pergreffi).

https://doi.org/10.1016/j.pnucene.2025.105940
Received 24 December 2024; Received in revised form 18 June 2025; Accepted 14 July 2025
Available online 19 July 2025

smaller in a fast reactor than in a thermal one due to the combination of two phenomena: the higher breeding ability, which better compensates fission losses, and the small contribution on reactivity of the fission products (FPs) due to low neutron-absorption cross sections in the fast spectrum [Evans, 2021]. For these reasons, the control of LMFBRs has been usually carried out with stainless-steel rods filled with boron carbide.

The present study stems from the need to identify promising candidates as burnable poisons for the technology of small – and notably micro – liquid-metal-cooled fast reactors. To this end, a model tailored for fast spectrum reactors was developed that estimates the neutronic behavior of a candidate without requiring extensive calculations, for which a detailed description of the system in terms of geometry and materials would be required. The model makes it possible to calculate numerical values that can be used in a comparison of materials to estimate their neutronic performances. In this sense, it can be considered as a semi-quantitative model. It is important to emphasize that this model is not intended to be an alternative to neutronic codes, but rather a tool to orient the design by identifying, through fast preliminary and approximate evaluations, the most promising materials as burnable poisons which then will need to be characterized on real configurations using conventional neutronic codes.

The model was tested with seven materials: Eu_2O_3, Gd_2O_3, Dy_2O_3, Er_2O_3, NpO_2, AmO_2 and B_4C. The rare-earth compounds were chosen being well-known in light water reactors (LWRs) [Asou, 1997], while the two minor actinide compounds were selected as they represent the most promising solutions for liquid metal fast reactors due to their initial negative contribution to the neutron balance that becomes less and less negative as burnup increases [Guo, 2019; Liu, 2020]. For an assessment of the model, a comparison was made with the detailed neutronic results obtained from simulations with MCNP6.1 [Goorley, 2013] for a lead-cooled fast reactor (LFR) fuel assembly (FA) with UO_2 fuel enriched in ^{235}U at 19.75 wt% in which, one at a time, the various candidates have been added: in particular, the first six materials were homogeneously mixed with UO_2 while B_4C was placed in dedicated pins.

It is worth noting that "neutronic behavior" is here to be understood as the effectiveness of a material in controlling the positive reactivity required to ensure the criticality of the system over a certain period of time. As it is well known, there are other requirements which a burnable poison must meet, including also those related to fabricability and cost or those (in-core requirements) related to the ability not to compromise the integrity of structural materials (for instance by swelling), nor degrade the thermomechanical properties of the fuel if they are mixed with it. Although these requirements are equally important as the neutronic ones, they are not taken into account by the present model, being beyond the scope of this study.

2. Methodology

The effectiveness of a burnable poison in controlling the positive reactivity over time can be seen as the combination of two distinct effects.

- provide at a given instant of time (generally, at beginning of cycle – BoC) an anti-reactivity such as to compensate for the excess reactivity of the fuel;
- have a burnup kinetics such as to balance the reactivity change due mainly to fuel depletion.

Note that while the first effect can, at least theoretically, be obtained with any material (in fact, in the case of low absorption cross sections, concentrations can be adjusted accordingly to provide the required anti-reactivity), the second effect is strictly dependent on the absorption cross sections of the isotopes formed by the neutron capture in the poison.

Based on this distinction, it is possible to associate the first effect with the attribute of 'poisonousness' and the second, related to the anti-reactivity provided as a function of time, with the attribute of 'burnability'.

The neutronic model developed in this study aims at estimating the effectiveness of a material by considering its neutronic performance in terms of poisonousness separately from that in terms of burnability. For each attribute, an equation has been written. In this regard, it should be pointed out that, since the model is designed to work without reference to a detailed configuration, the effective microscopic cross sections to be used in these equations need not be specifically related to the configuration under examination but need only be representative of the spectral conditions of the system taken as reference. In other words, approximate cross sections (i.e., calculated using a neutron spectrum that is representative of the system of interest) are to be used.

A description of these equations is provided in the sections below.

2.1. Poisonousness

The performance in terms of poisonousness is estimated through Eq. (1) which relates the (negative) contribution on the neutron balance of a given poison to that (positive) of the fissile material at time t_0:

$$e_{POIS} = \frac{\sum_i A_i(0)\left(\nu\sigma_f - \sigma_a\right)_i \phi_P}{\sum_j A_j(0)\left(\nu\sigma_f - \sigma_a\right)_j \phi_F} \tag{1}$$

In Eq. (1), the subscripts i and j refer respectively to poison and fissile isotopes, σ_f and σ_a are the fission and absorption one-group effective cross sections, ν is the average number of neutrons generated per fission event, $A(0)$ is the abundance, in atom fraction, of a given isotope at time t_0 and, finally, ϕ_P and ϕ_F are average scalar fluxes in the poison and fuel, respectively. The term $\left(\nu\sigma_f - \sigma_a\right)$ is used to account for the net contribution to the neutron balance, that is, the net number of neutrons introduced in the system by each isotope. Moreover, to appreciate the effective contribution of a material, this ratio is done in terms of microscopic cross sections, that is, without considering the atom density of the material itself.

If we define the ratio of the average flux in the poison region – ϕ_P – to the average flux in the fuel region – ϕ_F – as the spatial self-shielding factor of the poison $f_{ss}(t)$ [Stacey, 2001] i.e.,

$$f_{ss} = \frac{\phi_P}{\phi_F} \tag{2}$$

Eq. (1) can be rewritten as follows:

$$e_{POIS} = f_{ss}\frac{\sum_i A_i(0)\left(\nu\sigma_f - \sigma_a\right)_i}{\sum_j A_j(0)\left(\nu\sigma_f - \sigma_a\right)_j} \tag{3}$$

The factor f_{ss} is exactly equal to 1 for a uniform distribution of poison inside the fuel i.e., when the poison is homogeneously mixed into the fuel, whereas it is lower than 1 with a heterogeneous distribution due to the phenomenon of spatial self-shielding of the poison. In fast reactors, however, since the mean free path is longer than the thickness of the absorber material, spatial self-shielding effects are usually less important and this factor can be assumed equal to 1.

It should be noted that, as a ratio of one-energy-group and spatial-independent reaction rates, the function e_{POIS} weighs net productions and removals without considering the real (energetic and spatial) importance of the produced or absorbed neutrons. To include this, as is well known, a ratio of reaction rates weighted by the adjoint flux should be used. However, this would require a detailed description of the system in terms of materials and geometry, which is exactly what we want to avoid with the model: for this, the model is kept simple, accepting to disregard any such additional considerations. As a consequence, when spatial or energetic effects play an important role, it should be kept in

Table 1
Application of Eq. (4) to the Superphénix fuel.

Isotope	σ_c [b]	σ_f [b]	ν [-]	$\nu\sigma_f - \sigma_a = x$ [b]	δx [b]	$\delta x \sigma_c = e$ [b^2]
Transmutation ^{237}Np → ^{238}Pu						
^{237}Np	1.79	0.31	3.01	−1.17	2.33	4.17
^{238}Pu	0.70	1.02	2.83	1.16		
Transmutation ^{238}U → ^{239}Pu						
^{238}U	0.31	0.041	2.81	−0.24	3.20	0.99
^{239}Pu	0.54	1.86	2.88	2.96		

mind that the prediction capability of this equation could be partially affected.

2.2. Burnability

The development of an equation to estimate the effectiveness of a material in terms of burnability takes the move from the neutronic model developed in [Pilate, 1988] to evaluate innovative solutions introduced in large LMFBR cores such as Superphénix and SNR-2 to reduce the burnup reactivity loss. In that work, to meet the requirement of increasing the burnup without relying further on control rods (which would aggravate the threat of CRW accidents and enlarge power tilts), the addition of ^{237}Np to the MOX fuel was considered. The physical basis of such idea is that, although ^{238}Pu is a less good fissile than ^{239}Pu, the conversion rate of ^{237}Np to ^{238}Pu is quicker than that of ^{238}U to ^{239}Pu. Therefore, transmutation from ^{237}Np inserted in the fuel instead of ^{238}U leads to an increase in positive reactivity over time. These physical considerations were confirmed by an equation that evaluates the effectiveness of a material – e – with the following equation:

$$e = \left[\left(\nu\sigma_f - \sigma_a\right)_d - \left(\nu\sigma_f - \sigma_a\right)_p\right](\sigma_c)_p \tag{4}$$

where σ_f, σ_a and σ_c are one-group effective cross sections (fission, absorption, and capture, respectively) and the subscripts d and p refer to the daughter and parent isotopes, respectively. The Eq. (4) is the product of two terms: the first estimates the reactivity variation due to a transmutation as a difference among the reactivity contributions of the daughter and parent isotopes of the transmutation itself, while the second, that is the capture cross section of the parent isotope, represents the probability that exactly that reaction takes place. Even if the function e has no physical meaning per se – its unit of measurement is in fact barn^2 –, its values, from multiple cases, can be compared with the greatest one corresponding to the case providing the largest reactivity swing reduction.

By setting:

$$\left(\nu\sigma_f - \sigma_a\right) = x \tag{5}$$

Eq. (4) becomes:

$$e = \left(x_d - x_p\right)(\sigma_c)_p = \delta x(\sigma_c)_p \tag{6}$$

The application of this equation to the case of the Superphénix reactor, as done in [Pilate, 1988], is reported, by way of example, in Table 1. The fuel composition was that typical of the inner zone of Superphénix with 84.2 wt% uranium (of which 99.55 % ^{238}U) and 15.8 wt% plutonium (with americium). The one-group cross sections were derived from a modified KfKINR1 cross-section set. By comparing the values of e related to the two transmutations (namely, ^{237}Np to ^{238}Pu and ^{238}U to ^{239}Pu) with the corresponding variations of k_{inf} over 2 years operation time (and a burnup of 62.7 MWd/kg) performed with the KORIGEN depletion code, it can be seen that the transmutation for which this value is larger is the one with the greater increase in positive reactivity over time.

Although referred to a very specific case in which only one transmutation is relevant for the change in reactivity, the idea behind this equation is consistent with the attribute of burnability. Eq. (4) was therefore used in this study as a starting point to develop a new equation that allows to estimate the performance of a material in terms of burnability in the most general case, that is, with materials with more than one isotope and with more complex evolution chains. From a physical point of view, this new equation is designed to calculate the anti-reactivity provided over time by the isotopes into which the initial isotopes evolve by transmutation or decay. Mathematically, it is as follows:

$$e_{BURN}(t) = \sum\nolimits_i [\delta x A_d(t)]_i \tag{7}$$

where the summation index i extents to all transmutations or decays in the BP evolution chain and A_d, that is expressed in atom fraction [%], is the total amount of the daughter isotope produced by a single event over time t. In this equation the term δx that estimates the change in reactivity due to each transmutation or decay is multiplied by A_d, this value being exactly equal to the total number of times that, over time t, that event occurs. In both terms, one-group cross sections are used. From a dimensional point of view, e_{BURN} is in barn [b], since the units of measurement of δx and A_d are, respectively, barn and a dimensionless quantity.

A_d is calculated in two steps. First, by solving the evolution equation of each parent isotope p so to know its quantity as a function of time, $A_p(t)$:

$$\frac{dA_p(t)}{dt} = \sum_{k\in BP}\left[\left(\lambda_{k\to p} + \sigma_a^{k\to p}\phi\right)A_k(t)\right] - \left(\lambda_p + \sigma_a^p\phi\right)A_p(t) \tag{8}$$

In Eq. (8), λ is the radioactive decay constant. It is worth noting that the k index in the production term must consider only those isotopes that belong to the BP chain. In general, the evolution equation takes into account any production or removal which, over a unit time interval, causes the concentration of a certain isotope to vary. In this case, however, the production of an isotope as a result of the transmutation or decay of isotopes which do not specifically depend on the initial quantities of the BP isotopes must not be taken into account, this production being independent of the BP itself.

As a second step, by integrating over time the event on which the production of a daughter isotope depends. If this event is a transmutation, the amount of the daughter isotope over time t is given by Eq. (9):

$$A_d(t) = \int \sigma_y \phi A_p(t')dt' \tag{9}$$

where the subscript y refers to a generic neutron reaction, while if this event is a radioactive decay, its amount is given by Eq. (10):

$$A_d(t) = \int \lambda A_p(t')dt' \tag{10}$$

With regard to the calculation of A_d, it is worth noting that, since Eq. (7) requires that the various transmutation or decay events be kept distinct, the quantities of any isotope d produced by different parents must also be kept distinct. Moreover, A_d needs always be net of its initial amount, if any.

Thus defined, A_d becomes rather complex to calculate in the case of fission reactions when a large number of daughter isotopes is produced by transmutation. To reduce this complexity, we take advantage of the fact that the impact of fission products on reactivity is small in fast reactors. Therefore, as a first approximation, the reactivity contribution due to the j-th fission product – x_j – can be neglected. In this way, A_d comes to be equal to the amount of the fissile isotope, hereinafter indicated with $A_{p_{fiss}}$, that undergoes fission reactions over time t. The contribution of fission reactions to burnability due to fissile isotopes can thus be calculated with the following equation:

$$\sum_f \left[\sum_j (x_j - x_p) A_{d_j}(t)\right]_f =$$
$$\sum_f \left[\sum_j \left((x_j - x_p)\int_0^t Y_j \sigma_f \phi A_p(t')dt'\right)\right]_f \cong$$
$$\sum_f \left[\sum_j \left(-x_p \int_0^t Y_j \sigma_f \phi A_p(t')dt'\right)\right]_f = \quad (11)$$
$$\sum_f \left[\sum_j Y_j \left(-x_p \int_0^t \sigma_f \phi A_p(t')dt'\right)\right]_f =$$
$$\sum_f \left[-x_p \int_0^t \sigma_f \phi A_p(t')dt'\right]_f = \sum_f \left[-x_p A_{p_{fiss}}(t)\right]_f$$

in which Y_j is the yield of fission product j (normalized so that all fractions sum to 1) and the summation indexes f and j extend to all fission reactions due to the fissile isotopes in the BP chain and to all fission products, respectively.

Therefore, if fissile isotopes are present in the burnable poison or in its evolution chain, the following equation replaces Eq. (7) for the calculation of burnability:

$$e_{BURN}(t) = \sum_r [\delta x A_d(t)]_r + \sum_f \left[-x_p A_{p_{fiss}}(t)\right]_f \quad (12)$$

where r denotes any decay or transmutation except fission reaction, and f denotes just the fission reactions.

In these equations, the cross sections should vary as a function of time. In fact, these are averages weighted on the neutron spectrum which varies with the variation of isotope concentrations. But, since in fast reactors the spectrum variations are relatively small, the constant cross section approximation can reasonably be introduced [Reuss, 2008].

The choice of the evolution chains is a crucial aspect of the model to be evaluated on a case-by-case basis. Of course, the accuracy of the burnability results strongly depends on the length of the chains i.e., on the number of isotopes included in the chains. In this regard, an isotope can be skipped in the chain only if it has a very short lifetime compared with the rate of transmutations. A chain ends only when one isotope is found in a very small quantity and its daughter isotopes have low absorption cross sections.

An example of burnability calculation is given in APPENDIX A for neptunium assumed as 100 % ^{237}Np.

2.3. Residual reactivity penalty

As is known, one of the crucial neutronic parameters for evaluating the performance of a burnable poison is the residual reactivity penalty, defined as the difference in reactivity of poisoned versus non-poisoned cases. From a theoretical point of view, the residual reactivity penalty can be seen as a combination of the poisonousness and burnability. In fact, intuitively, materials with low poisonousness and high burnability should have a low residual reactivity penalty, while materials with high poisonousness and low burnability should have a high residual penalty. In Chapter 6, an equation will be shown that, by combining these two quantities, is able to provide information about the behavior of a material in terms of residual reactivity penalty.

3. Neutronic code

The subsequent two phases of testing and assessing the model have required calculations performed with the general-purpose Monte Carlo radiation-transport code MCNP6.1. In both phases, the ENDF/B-VIII.0 distribution [Brown, 2018] processed by LANL in ACE format [Conlin, 2018] was chosen as evaluated nuclear data library. Effective cross sections were calculated as follows.

- first, by applying a tally multiplier (FM) to a standard flux tally (F4) on the unit volume of the region of interest fictitiously filled with the only isotope for which the reaction rate in a certain energy range is calculated;
- secondly, by multiplying this result by a normalization factor, being the FM-multiplied tally given in units of MeV-barn/cm^2 per source neutron;
- finally, by dividing the latter value by the flux in that energy range.

In the assessment phase, all depletion calculations were performed with MCNP6.1 by including all fission products in the ENDF/B-VII.0 library that have yield information for CINDER90 (the depletion code implemented in MCNP6.1).

All calculations were performed on CRESCO6, the Linux cluster with 434 interconnected nodes integrated into the ENEAGRID infrastructure [Iannone, 2019].

Table 2
Initial atom fractions of the main isotopes.

Material	Isotope	Atom fraction in the element	Atom fraction in the material
B_4C	^{10}B	0.1990	0.1592
Eu_2O_3	^{151}Eu	0.4780	0.1912
	^{153}Eu	0.5220	0.2088
Gd_2O_3	^{154}Gd	0.0218	0.0087
	^{155}Gd	0.1480	0.0592
	^{156}Gd	0.2047	0.0819
	^{157}Gd	0.1565	0.0626
	^{158}Gd	0.2484	0.0994
	^{160}Gd	0.2186	0.0874
Dy_2O_3	^{160}Dy	0.0233	0.0093
	^{161}Dy	0.1889	0.0756
	^{162}Dy	0.2548	0.1019
	^{163}Dy	0.2490	0.0996
	^{164}Dy	0.2826	0.1130
Er_2O_3	^{164}Er	0.0160	0.0064
	^{166}Er	0.3350	0.1340
	^{167}Er	0.2287	0.0915
	^{168}Er	0.2698	0.1079
	^{170}Er	0.1491	0.0596
NpO_2	^{237}Np	1.0000	0.3333
AmO_2	^{241}Am	0.7500	0.2500
	^{243}Am	0.2500	0.0833

4. Test phase

This model was tested with the following materials: Eu_2O_3, Gd_2O_3, Dy_2O_3, Er_2O_3, NpO_2, AmO_2 and B_4C. The initial atom fractions of the main isotopes in both the element and material are given in Table 2.

All elements were considered with their natural abundance according to NIST standard reference data [Coursey, 2015] except neptunium considered as 100 % ^{237}Np and americium considered as 75 % ^{241}Am and 25 % ^{243}Am (these percentages are taken arbitrarily for demonstration purposes).

The depletion chains of Eu, Gd, Dy, Er, Np and Am are illustrated in Fig. 1 along with that of U. These chains are simplified in that they include neither the fission products of fissile isotopes (where present) nor isotopes whose actual contribution to the change in reactivity has been calculated to be negligible. Moreover, ^{165}Dy in the dysprosium depletion chain and ^{171}Er and ^{172}Er in the erbium depletion chain are not included as they are absent in the library ENDF/B-VIII.0. It should be also noted that the empty boxes in Fig. 1 represent isotopes with a very short decay time and can therefore be neglected in the evolution calculation.

For each isotope in Fig. 1, the one-group effective cross sections used in the model equations were calculated with MCNP6 for a hexagonal cell with UO_2 fuel and lead coolant. All geometrical and material details,

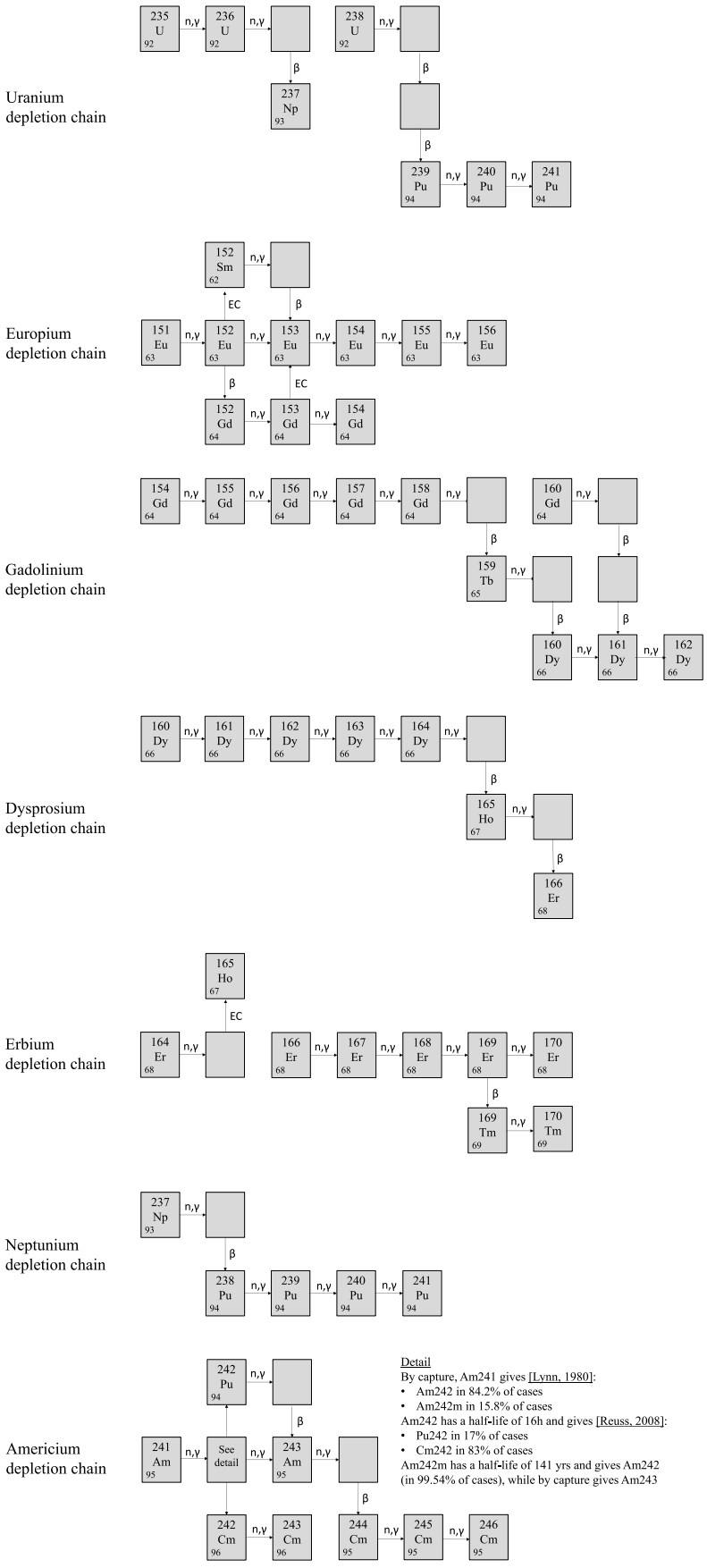

Fig. 1. Simplified transmutation-decay chains of U, Eu, Gd, Dy, Er, Np and Am (Lynn et al., 1980).

Table 3
One-group effective cross sections [barn].

Isotope	σ_f	ν	$\sigma_{(n,\alpha)}$	$\sigma_{(n,\gamma)}$	σ_a
^{10}B			2.18E+00	2.32E-04	2.20E+00
^{152}Sm				2.92E-01	2.92E-01
^{151}Eu				2.36E+00	2.36E+00
^{152}Eu				2.93E+00	2.93E+00
^{153}Eu				1.68E+00	1.68E+00
^{154}Eu				2.15E+00	2.15E+00
^{155}Eu				7.27E-01	7.27E-01
^{156}Eu				3.87E-01	3.87E-01
^{152}Gd				7.36E-01	7.36E-01
^{153}Gd				1.64E+00	1.64E+00
^{154}Gd				6.56E-01	6.56E-01
^{155}Gd				1.61E+00	1.61E+00
^{156}Gd				4.03E-01	4.03E-01
^{157}Gd				8.76E-01	8.76E-01
^{158}Gd				1.97E-01	1.97E-01
^{160}Gd				1.03E-01	1.03E-01
^{159}Tb				1.29E+00	1.29E+00
^{160}Dy				5.61E-01	5.61E-01
^{161}Dy				1.19E+00	1.19E+00
^{162}Dy				2.92E-01	2.92E-01
^{163}Dy				6.76E-01	6.76E-01
^{164}Dy				1.38E-01	1.38E-01
^{165}Ho				8.45E-01	8.45E-01
^{164}Er				1.31E+00	1.31E+00
^{166}Er				4.13E-01	4.13E-01
^{167}Er				9.52E-01	9.52E-01
^{168}Er				1.74E-01	1.74E-01
^{169}Er				4.14E-01	4.14E-01
^{170}Er				1.29E-01	1.29E-01
^{169}Tm				7.07E-01	7.07E-01
^{170}Tm				1.17E+00	1.17E+00
^{235}U	1.69E+00	2.46		4.44E-01	2.13E+00
^{236}U	9.39E-02	2.63		3.63E-01	3.63E-01
^{238}U	3.96E-02	2.72		2.37E-01	2.77E-01
^{237}Np	3.41E-01	2.85		1.30E+00	1.64E+00
^{238}Pu	1.05E+00	3.02		5.07E-01	1.56E+00
^{239}Pu	1.68E+00	2.94		3.64E-01	2.04E+00
^{240}Pu	3.79E-01	3.03		4.02E-01	7.81E-01
^{241}Pu	2.23E+00	2.97		3.54E-01	2.58E+00
^{242}Pu	2.68E-01	3.10		3.33E-01	6.02E-01
^{241}Am	2.60E-01	3.36		1.57E+00	1.83E+00
^{242m}Am	2.87E+00	3.32		3.95E-01	3.26E+00
^{243}Am	1.90E-01	3.53		1.39E+00	1.58E+00
^{242}Cm	6.93E-01	3.43		6.45E-01	1.34E+00
^{243}Cm	3.03E+00	3.48		2.99E-01	3.33E+00
^{244}Cm	4.75E-01	3.63		4.83E-01	9.58E-01
^{245}Cm	2.39E+00	3.62		3.69E-01	2.76E+00
^{246}Cm	2.90E-01	3.81		2.91E-01	5.82E-01

Table 4
Poisonousness [-] at the initial time.

Material	ε_{POIS}
Eu_2O_3	−9.0
Gd_2O_3	−2.4
Dy_2O_3	−2.3
Er_2O_3	−2.0
NpO_2	−2.5
AmO_2	−3.5
B_4C	−3.9

together with the main calculation settings, are given in APPENDIX B. Since the reaction rates refer to an undoped configuration, that is, one in which the spectrum is not affected by the presence of the burnable poison, these are approximate values.

From the values in Table 3, it can be seen that the absorption cross sections basically coincide, as expected, with the radiative capture cross sections for the rare-earth isotopes, (n,α) reaction cross section for ^{10}B and the sum of fission and radiative capture cross sections for the actinides.

Table 5
Atom fractions of the daughter isotopes A_d [%] over increasing irradiation times [years].

Isotope	5 y	10 y	15 y	20 y	30 y	50 y
Depletion chain of uranium						
^{236}U	0.002	0.003	0.004	0.006	0.007	0.010
^{237}Np	0.000	0.000	0.000	0.000	0.001	0.001
^{239}Pu	0.004	0.007	0.011	0.015	0.021	0.035
^{240}Pu	0.000	0.000	0.000	0.001	0.001	0.003
^{241}Pu	0.000	0.000	0.000	0.000	0.000	0.000
Depletion chain of europium						
^{152}Eu	0.025	0.047	0.066	0.082	0.109	0.144
^{153}Eu(^{152}Eu)	0.002	0.006	0.012	0.019	0.031	0.050
^{153}Eu(^{153}Gd)	0.000	0.000	0.000	0.001	0.001	0.004
^{153}Eu(^{152}Sm)	0.000	0.000	0.000	0.001	0.001	0.004
^{154}Eu	0.020	0.038	0.055	0.071	0.101	0.150
^{155}Eu	0.001	0.004	0.007	0.010	0.018	0.031
^{156}Eu	0.000	0.000	0.000	0.000	0.001	0.001
^{152}Sm	0.002	0.007	0.013	0.020	0.033	0.053
^{152}Gd	0.001	0.003	0.005	0.008	0.013	0.020
^{153}Gd	0.000	0.000	0.000	0.001	0.001	0.004
^{154}Gd	0.000	0.000	0.000	0.000	0.000	0.000
Depletion chain of gadolinium						
^{155}Gd	0.000	0.001	0.001	0.001	0.002	0.003
^{156}Gd	0.004	0.010	0.015	0.019	0.026	0.036
^{157}Gd	0.002	0.004	0.006	0.008	0.013	0.023
^{158}Gd	0.003	0.006	0.010	0.013	0.019	0.030
^{159}Tb	0.001	0.002	0.004	0.005	0.007	0.013
^{160}Dy	0.000	0.000	0.000	0.001	0.001	0.004
^{161}Dy(^{160}Dy)	0.000	0.000	0.000	0.000	0.000	0.000
^{161}Dy(^{160}Gd)	0.001	0.001	0.002	0.002	0.003	0.005
^{162}Dy	0.000	0.000	0.000	0.000	0.001	0.001
Depletion chain of dysprosium						
^{161}Dy	0.001	0.001	0.002	0.002	0.003	0.005
^{162}Dy	0.005	0.010	0.014	0.019	0.026	0.038
^{163}Dy	0.002	0.004	0.006	0.008	0.012	0.020
^{164}Dy	0.004	0.008	0.012	0.015	0.023	0.036
^{165}Ho	0.001	0.002	0.003	0.004	0.006	0.010
^{166}Er	0.000	0.000	0.000	0.000	0.001	0.002
Depletion chain of erbium						
^{165}Ho	0.000	0.001	0.001	0.002	0.002	0.003
^{167}Er	0.003	0.006	0.010	0.013	0.018	0.029
^{168}Er	0.005	0.010	0.015	0.020	0.029	0.047
^{169}Er	0.001	0.002	0.004	0.005	0.007	0.013
^{170}Er	0.000	0.000	0.000	0.000	0.000	0.000
^{169}Tm	0.001	0.002	0.004	0.005	0.007	0.013
^{170}Tm	0.000	0.000	0.000	0.000	0.001	0.002
Depletion chain of neptunium						
^{238}Pu	0.025	0.047	0.067	0.085	0.117	0.164
^{239}Pu	0.000	0.001	0.003	0.005	0.010	0.021
^{240}Pu	0.000	0.000	0.000	0.000	0.000	0.001
^{241}Pu	0.000	0.000	0.000	0.000	0.000	0.000
Depletion chain of americium						
^{242m}Am	0.003	0.007	0.009	0.012	0.016	0.022
^{243}Am(^{242m}Am)	0.000	0.000	0.000	0.000	0.001	0.002
^{243}Am(^{242}Pu)	0.000	0.000	0.000	0.000	0.001	0.002
^{242}Pu	0.003	0.006	0.008	0.011	0.014	0.020
^{242}Cm	0.015	0.029	0.041	0.052	0.070	0.096
^{243}Cm	0.000	0.000	0.000	0.000	0.000	0.000
^{244}Cm	0.007	0.013	0.018	0.023	0.032	0.045
^{245}Cm	0.000	0.000	0.001	0.001	0.002	0.004
^{246}Cm	0.000	0.000	0.000	0.000	0.000	0.000
Depletion chain of boron						
^{7}Li	0.019	0.036	0.051	0.064	0.086	0.115

4.1. Poisonousness

The poisonousness value at time t_0 is given for each material in Table 4. The ranking was found as follows: Eu_2O_3, B_4C, AmO_2, NpO_2, Gd_2O_3, Dy_2O_3, Er_2O_3. Eu, which is known to have absorption cross sections in the fast spectrum comparable to that of ^{10}B for both naturally occurring isotopes [Cinotti, 2010] proved to be the most promising material in terms of poisonousness, followed by B and Am. Np, Dy, Gd and Er, whose performances are very similar, close the ranking.

Table 6
Atom fractions of the parent fissile isotopes $A_{p_{fiss}}$ [%] over increasing irradiation times [years].

Isotope	5 y	10 y	15 y	20 y	30 y	50 y
Depletion chain of uranium						
^{235}U	0.006	0.012	0.017	0.021	0.028	0.038
^{237}Np	0.000	0.000	0.000	0.000	0.000	0.000
^{238}U	0.001	0.001	0.002	0.002	0.004	0.006
^{239}Pu	0.000	0.001	0.001	0.003	0.005	0.012
^{240}Pu	0.000	0.000	0.000	0.000	0.000	0.000
^{241}Pu	0.000	0.000	0.000	0.000	0.000	0.000
Depletion chain of neptunium						
^{237}Np	0.006	0.012	0.018	0.022	0.031	0.043
^{238}Pu	0.001	0.003	0.006	0.010	0.020	0.044
^{239}Pu	0.000	0.000	0.000	0.001	0.002	0.006
^{240}Pu	0.000	0.000	0.000	0.000	0.000	0.000
Depletion chain of americium						
^{241}Am	0.004	0.007	0.010	0.012	0.017	0.023
^{242m}Am	0.000	0.001	0.002	0.003	0.006	0.011
^{243}Am	0.001	0.002	0.002	0.003	0.004	0.006
^{242}Pu	0.000	0.000	0.000	0.000	0.001	0.002
^{242}Cm	0.000	0.000	0.000	0.000	0.000	0.001
^{243}Cm	0.000	0.000	0.000	0.000	0.000	0.000
^{244}Cm	0.000	0.000	0.001	0.001	0.002	0.004
^{245}Cm	0.000	0.000	0.000	0.000	0.000	0.001

Table 7
Burnability [barn] at increasing irradiation times [years].

Material	5 y	10 y	15 y	20 y	30 y	50 y
UO_2 (ref.)	−0.006	−0.011	−0.02	−0.02	−0.03	−0.04
Eu_2O_3	−0.013	−0.008	0.006	0.025	0.064	0.127
Gd_2O_3	0.006	0.012	0.017	0.021	0.029	0.040
Dy_2O_3	0.005	0.010	0.014	0.018	0.025	0.037
Er_2O_3	0.002	0.004	0.005	0.007	0.010	0.014
NpO_2	0.060	0.112	0.158	0.198	0.262	0.340
AmO_2	0.070	0.129	0.179	0.222	0.289	0.374
B_4C	0.043	0.080	0.113	0.142	0.189	0.254

Table 8
Average fluxes with a poison content in the doped cases of 1.5 at.%.

Case	Flux [$cm^{-2}{\cdot}s^{-1}$]	Rel. Diff. [%]
UO_2 (ref.)	3.77E+14	–
$(U,Eu)O_2$	3.87E+14	+2.68
$(U,Gd)O_2$	3.83E+14	+1.60
$(U,Dy)O_2$	3.83E+14	+1.58
$(U,Er)O_2$	3.83E+14	+1.57
$(U,Np)O_2$	3.74E+14	−0.85
$(U,Am)O_2$	3.76E+14	−0.36
UO_2+B_4C	3.81E+14	+0.89

4.2. Burnability

The atom fractions of the daughter isotopes (A_d) and those of the parent fissile isotopes undergoing fission reactions ($A_{p_{fiss}}$) over increasing irradiation times are shown in Tables 5 and 6, respectively. It is worth remembering that for the isotopes present in the initial compositions of the materials, the atom fractions are always net of the initial ones. In Table 5, the atom fractions of the isotopes ^{153}Eu, ^{161}Dy and ^{243}Am are given by distinguishing the reactions from which they derive. In this regard, the parent isotopes are reported in brackets.

It is very important to note that the values in both Tables were calculated using the same flux and time steps for the different materials. In particular, a flux value of 3.77E+14 cm^{-2} s^{-1} was used which is, for convenience, the average flux over the whole irradiation period of the case with only UO_2 (reference case) calculated with MCNP6 for assessment purposes (see Table 8 in the next paragraph).

The choice of using the same flux and time steps for all materials stems from the fact that the model is designed to be used in the absence of well-defined configurations. At the same time, this choice does not take into account that, as the materials change, the fluxes to ensure the same powers and the times to reach exactly the same burnups are forced to change. As consequence, the model results are not fully comparable with each other. However, it was verified that the atom fractions calculated with the power and burnup values used in the assessment phase for the different cases deviated slightly from those reported in Tables 5 and 6.

Burnability at increasing irradiation times is given in Table 7 for the doped materials and undoped reference material. To better appreciate their evolution, the values have also been plotted in Fig. 2. As can be seen, AmO_2 NpO_2 and B_4C are always the most promising materials, followed by Eu_2O_3 but only from irradiation period longer than about 20 years. No relevant differences are found between Gd_2O_3 and Dy_2O_3, while Er_2O_3 is the least promising candidate.

5. Assessment phase

The results of the test phase needed to be assessed. Since there is no way to calculate the same quantities with codes, the assessment was not done on absolute values, but on the ranking derived from these, by comparing.

- the poisonousness as derived from the model, with the reduction in the initial criticality compared with the undoped case (as retrieved from the simulations);
- the burnability as derived from the model, with the reduction in the reactivity swing calculated as the difference between the multiplication factor at a certain time and that at the initial time (as retrieved from the simulations).

The following cases were simulated with MCNP6.1 for a typical LFR FA.

- one undoped case with only UO_2 (reference case);
- seven doped cases of which:
  - six homogeneous configurations i.e., $(U,Eu)O_2$, $(U,Gd)O_2$, $(U,Dy)O_2$, $(U,Er)O_2$, $(U,Np)O_2$ and $(U,Am)O_2$ with fuel and poison mixed together homogeneously in all FA pins;
  - one heterogeneous configuration i.e., with the fuel rods of UO_2 and the poisoned rods of B_4C arranged in different FA lattice positions.

In all cases, the isotopic composition of the uranium vector is the same as the one used in the test phase, with UO_2 enriched in ^{235}U at 19.75 wt%. Moreover, to ensure an equal comparison between the cases, the following conditions were applied.

- the total number of fuel and poison molecules in the doped cases was kept the same as that of uranium oxide in the reference case;
- the number of poison molecules in the seven doped cases was kept the same.

To assess how much the prediction ability of the model is affected by the poison content, the assessment was carried out for two values, namely 1.5 and 10 at.%. For the two heterogeneous cases with B_4C, the absorber rods have been located in the FAs so as to minimize their shadowing effect.

All geometrical and material details and the main calculation settings are given in APPENDIX C.

The main results of the assessment phase are described below. In this regard, it should be kept in mind that the burnability results of the model, being calculated by using the same average flux and time steps for all materials, correspond to slightly different burnup values from those fixed in the simulations with both poison contents (see APPENDIX C). However, these differences do not compromise their order, which

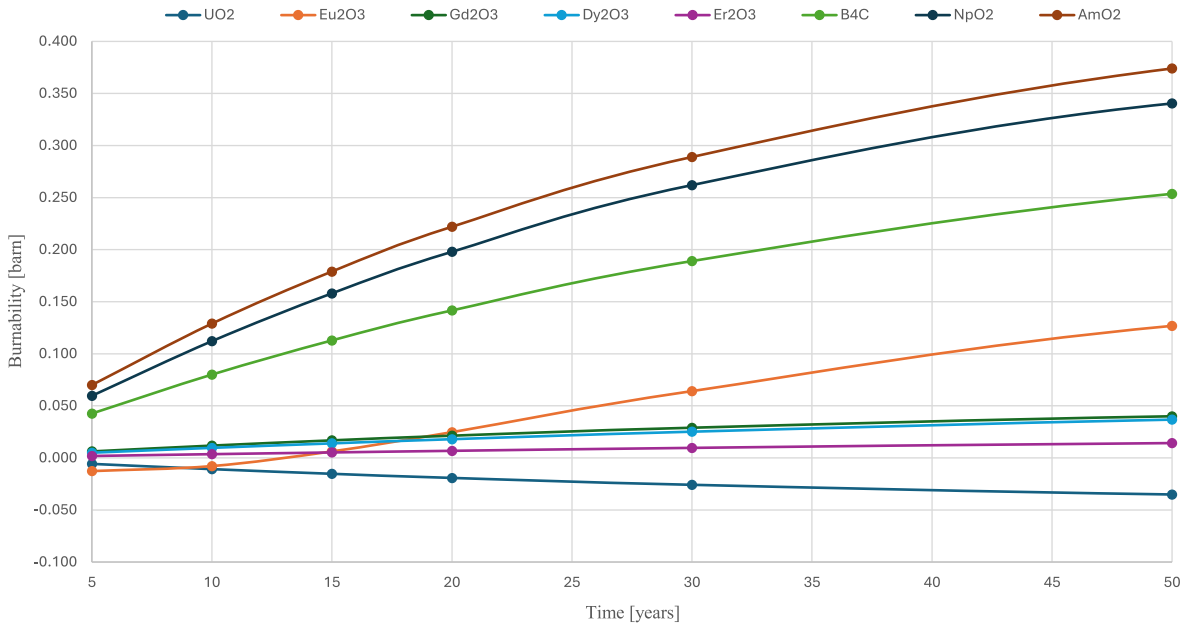

Fig. 2. Trend of burnability as a function of time for each material.

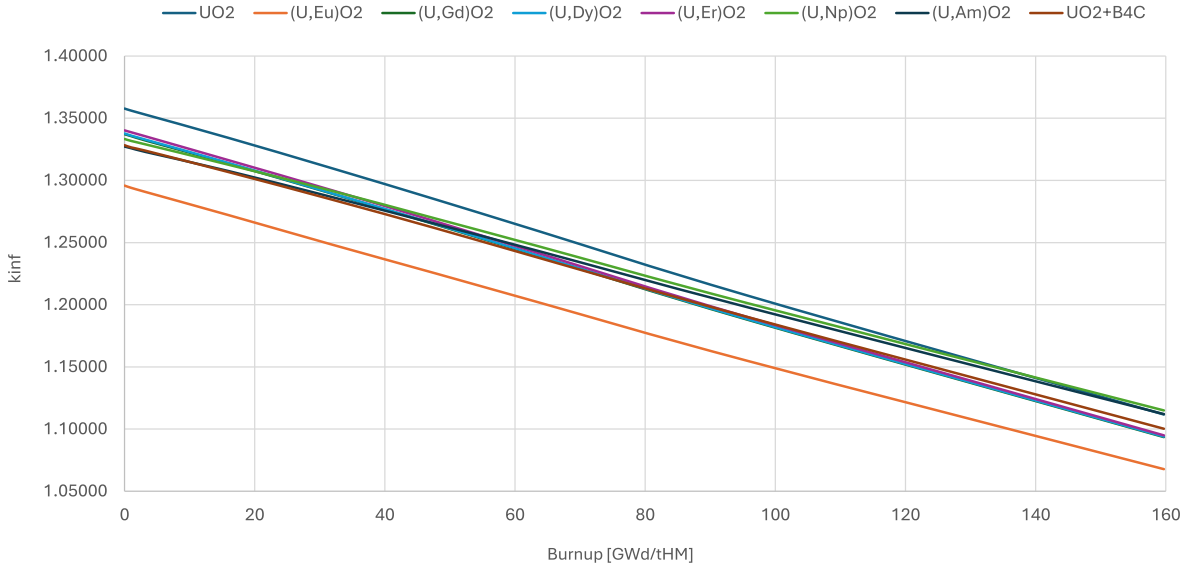

Fig. 3. Infinite multiplication factors as a function of burnup [GWd/t_{HM}] with a poison content in the doped cases of 1.5 at.%.

depends very weakly on these small burnup variations.

5.1. *Assessment for 1.5 at.% poison content*

The results for a poison content of 1.5 at.% are discussed here.

The infinite multiplication factors as a function of burnup of all eight cases are shown in Fig. 3. The relative error at one standard deviation of the criticality values never exceeds 14 pcm.

The average flux value over the corresponding depletion period (i.e., after a burnup of 159.71 GWd/t_{HM}) is reported for each case in Table 8. It is interesting to observe that the fluxes in the cases with neptunia and americia are lower than that of the reference case with only UO_2 (negative relative differences) due to the fission inventories that increase more over time.

5.1.1. *Poisonousness*

The infinite multiplication factors at beginning of life (BoL) for all cases (doped and undoped) and the reductions in the initial criticality of the doped cases versus the undoped case (UO_2) are shown in Table 9. From these values, the following order is found: Eu_2O_3, AmO_2, B_4C, NpO_2, Gd_2O_3, Dy_2O_3, Er_2O_3. Comparing it with the order deduced from

Table 9
Infinite multiplication factors at BoL with a poison content in the doped cases of 1.5 at.%.

Case	k_{inf} [-]	Δk_{inf} [pcm]
UO_2 (ref.)	1.35779	–
$(U,Eu)O_2$	1.29582	−6197
$(U,Gd)O_2$	1.33717	−2062
$(U,Dy)O_2$	1.33777	−2002
$(U,Er)O_2$	1.34023	−1756
$(U,Np)O_2$	1.33330	−2449
$(U,Am)O_2$	1.32722	−3057
UO_2+B_4C	1.32831	−2948

Table 10
Reactivity swings [pcm] at different burnups [GWd/t_{HM}] with a poison content in the doped cases of 1.5 at.%.

Case	15.97	31.94	47.91	63.89	95.83	159.71
UO_2 (ref.)	−2360	−4813	−7330	−9902	−15057	−24609
$(U,Eu)O_2$	−2372	−4754	−7080	−9431	−14110	−22807
$(U,Gd)O_2$	−2361	−4793	−7288	−9844	−14937	−24363
$(U,Dy)O_2$	−2375	−4826	−7312	−9863	−14954	−24386
$(U,Er)O_2$	−2397	−4827	−7341	−9917	−15033	−24532
$(U,Np)O_2$	−2069	−4181	−6413	−8668	−13218	−21832
$(U,Am)O_2$	−1969	−4072	−6233	−8440	−12937	−21517
UO_2+B_4C	−2160	−4387	−6697	−9094	−13830	−22807

Table 11
Comparison at different burnups [GWd/t_{HM}] between the order of MCNP results with a poison content in the doped cases of 1.5 at.% and the order of model results.

Case	15.97	31.94	47.91	63.89	95.83	159.71
Simulations (MCNP)						
Best	AmO_2	AmO_2	AmO_2	AmO_2	AmO_2	AmO_2
2	NpO_2	NpO_2	NpO_2	NpO_2	NpO_2	NpO_2
3	B_4C	B_4C	B_4C	B_4C	B_4C	B_4C
4	**Ref.**	Eu_2O_3	Eu_2O_3	Eu_2O_3	Eu_2O_3	Eu_2O_3
5	Gd_2O_3	Gd_2O_3	Gd_2O_3	Gd_2O_3	Gd_2O_3	Gd_2O_3
6	Eu_2O_3	**Ref.**	Dy_2O_3	Dy_2O_3	Dy_2O_3	Dy_2O_3
7	Dy_2O_3	Dy_2O_3	**Ref.**	**Ref.**	Er_2O_3	Er_2O_3
Worst	Er_2O_3	Er_2O_3	Er_2O_3	Er_2O_3	**Ref.**	**Ref.**
Model						
Best	AmO_2	AmO_2	AmO_2	AmO_2	AmO_2	AmO_2
2	NpO_2	NpO_2	NpO_2	NpO_2	NpO_2	NpO_2
3	B_4C	B_4C	B_4C	B_4C	B_4C	B_4C
4	Gd_2O_3	Gd_2O_3	Gd_2O_3	Eu_2O_3	Eu_2O_3	Eu_2O_3
5	Dy_2O_3	Dy_2O_3	Dy_2O_3	Gd_2O_3	Gd_2O_3	Gd_2O_3
6	Er_2O_3	Er_2O_3	Eu_2O_3	Dy_2O_3	Dy_2O_3	Dy_2O_3
7	**Ref.**	Eu_2O_3	Er_2O_3	Er_2O_3	Er_2O_3	Er_2O_3
Worst	Eu_2O_3	**Ref.**	**Ref.**	**Ref.**	**Ref.**	**Ref.**

Table 4, there is very good agreement. In fact, the two orders are completely overlapping except for the inversion between the cases with AmO_2 and B_4C, most likely due to the limitation of Eq. (3) that is not able to take into account the spatial self-shielding of boron. However, these two cases are very close, their discrepancy being 111 pcm with a statistical uncertainty of the calculations of 40 pcm (3σ). Furthermore, this discrepancy is still such that it does not compromise the assessment that can be drawn from the model results.

Table 12
Average fluxes with a poison content in the doped cases of 10 at.%.

Case	Flux [$cm^{-2}\cdot s^{-1}$]	Rel. Diff. [%]
UO_2 (ref.)	3.77E+14	–
$(U,Eu)O_2$	4.43E+14	+17.39
$(U,Gd)O_2$	4.21E+14	+11.59
$(U,Dy)O_2$	4.20E+14	+11.42
$(U,Er)O_2$	4.20E+14	+11.38
$(U,Np)O_2$	3.56E+14	−5.58
$(U,Am)O_2$	3.67E+14	−2.81
UO_2+B_4C	4.13E+14	+9.50

5.1.2. *Burnability*

The reactivity swing values at increasing burnup steps for the different cases are given in Table 10. From these values, it can be seen that the order of the three best cases, that is, those in which the reactivity swing is smaller, is the same regardless of the burnup value. This is not true for the worst cases for which the order, especially at lower burnups, is not preserved. However, these cases are often not neutronically distinguishable from each other, since the discrepancies between their reactivity swing values at a given burnup fall within the statistical uncertainty of the calculations. Specifically, this occurs with the five worst cases at burnups of 15.97 and 31.94 GWd/t_{HM} and with the four worst cases (so except Eu_2O_3) at burnups of 47.91, 63.89 and 95.83 GWd/t_{HM}.

The order of the results obtained with MCNP6.1 is compared with that of the model results in Table 11. About this comparison, the following is observed.

- for burnups lower than 47.91 GWd/t_{HM}, while an excellent agreement is observed for AmO_2, Np_2O and B_4C in the top three positions, some differences are found for the other materials. In fact, the model on the one hand overestimates the effectiveness for Gd_2O_3, Dy_2O_3 and Er_2O_3 (although their reciprocal positions are correct), and on the other hand underestimates the effectiveness of Eu_2O_3 (even if a correct, although not in phase, trend is shown as burnup increases);
- for burnups above 63.89 GWd/t_{HM}, excellent agreement is observed. In fact, except for the inversion between Er_2O_3 and UO_2 at 63.89 GWd/t_{HM}, the order is fully respected.

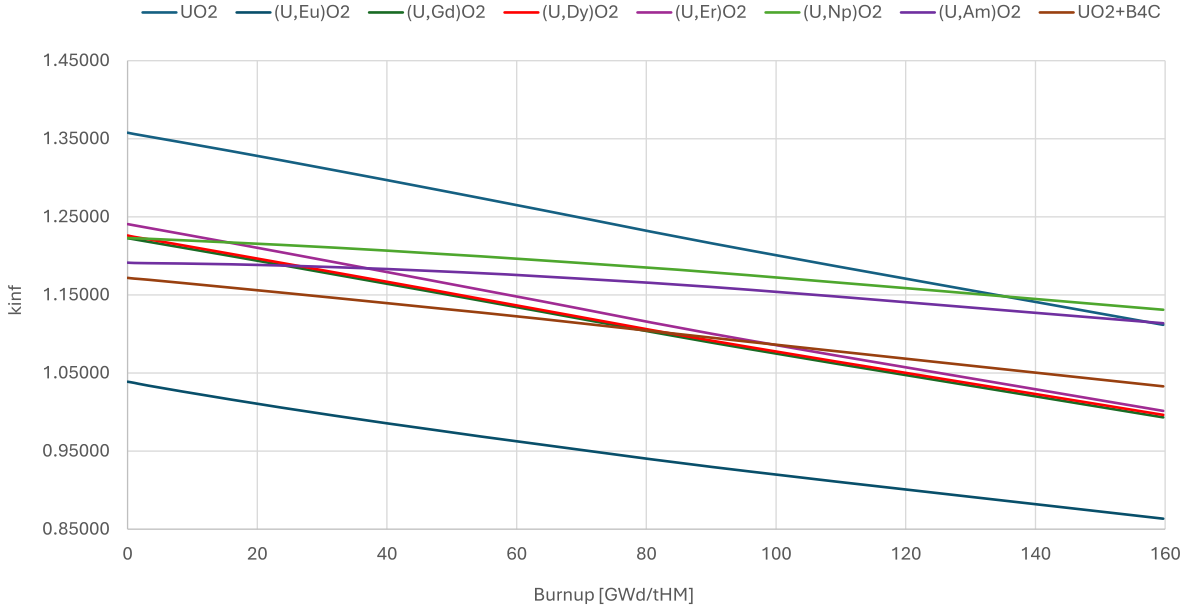

Fig. 4. Infinite multiplication factors as a function of burnup [GWd/t_{HM}] with a poison content in the doped cases of 10 at.%.

Table 13
Infinite multiplication factors at BoL of all cases with a poison content in the doped cases of 10 at.%.

Case	k_{inf} [-]	Δk_{inf} [pcm]
UO_2 (ref.)	1.35779	–
$(U,Eu)O_2$	1.03885	−31894
$(U,Gd)O_2$	1.22272	−13507
$(U,Dy)O_2$	1.22614	−13165
$(U,Er)O_2$	1.24075	−11704
$(U,Np)O_2$	1.22300	−13479
$(U,Am)O_2$	1.19138	−16641
UO_2+B_4C	1.17186	−18593

Table 14
Reactivity swings [pcm] at different burnups [GWd/t_{HM}] with a poison content in the doped cases of 10 at.%.

Case	15.97	31.94	47.91	63.89	95.83	159.71
UO_2 (ref.)	−2360	−4813	−7330	−9902	−15057	−24609
$(U,Eu)O_2$	−2287	−4351	−6248	−8059	−11487	−17544
$(U,Gd)O_2$	−2295	−4652	−7017	−9420	−14198	−22953
$(U,Dy)O_2$	−2360	−4730	−7115	−9545	−14281	−22979
$(U,Er)O_2$	−2416	−4885	−7386	−9887	−14896	−23931
$(U,Np)O_2$	−585	−1244	−2030	−2874	−4776	−9200
$(U,Am)O_2$	−216	−580	−1104	−1769	−3472	−7765
UO_2+B_4C	−1258	−2566	−3906	−5266	−8190	−13895

Table 15
Comparison at different burnups [GWd/t_{HM}] between the order of MCNP results with a poison content in the doped cases of 10 at.% and the order of model results.

Case	15.97	31.94	47.91	63.89	95.83	159.71
Simulations (MCNP)						
Best	AmO_2	AmO_2	AmO_2	AmO_2	AmO_2	AmO_2
2	NpO_2	NpO_2	NpO_2	NpO_2	NpO_2	NpO_2
3	B_4C	B_4C	B_4C	B_4C	B_4C	B_4C
4	Eu_2O_3	Eu_2O_3	Eu_2O_3	Eu_2O_3	Eu_2O_3	Eu_2O_3
5	Gd_2O_3	Gd_2O_3	Gd_2O_3	Gd_2O_3	Gd_2O_3	Gd_2O_3
6	Dy_2O_3	Dy_2O_3	Dy_2O_3	Dy_2O_3	Dy_2O_3	Dy_2O_3
7	**Ref.**	**Ref.**	**Ref.**	Er_2O_3	Er_2O_3	Er_2O_3
Worst	Er_2O_3	Er_2O_3	Er_2O_3	**Ref.**	**Ref.**	**Ref.**
Model						
Best	AmO_2	AmO_2	AmO_2	AmO_2	AmO_2	AmO_2
2	NpO_2	NpO_2	NpO_2	NpO_2	NpO_2	NpO_2
3	B_4C	B_4C	B_4C	B_4C	B_4C	B_4C
4	Gd_2O_3	Gd_2O_3	Gd_2O_3	Eu_2O_3	Eu_2O_3	Eu_2O_3
5	Dy_2O_3	Dy_2O_3	Dy_2O_3	Gd_2O_3	Gd_2O_3	Gd_2O_3
6	Er_2O_3	Er_2O_3	Eu_2O_3	Dy_2O_3	Dy_2O_3	Dy_2O_3
7	**Ref.**	Eu_2O_3	Er_2O_3	Er_2O_3	Er_2O_3	Er_2O_3
Worst	Eu_2O_3	**Ref.**	**Ref.**	**Ref.**	**Ref.**	**Ref.**

5.2. Assessment for 10 at.% poison content

The results with a poison content of 10 at.% are discussed here.

The infinite multiplication factors as a function of burnup for the different cases are shown in Fig. 4. The relative error at one standard deviation of the criticality values never exceeds 14 pcm.

The average flux values calculated over the entire irradiation periods (i.e., after a burnup of 159.71 GWd/t_{HM}) are reported in Table 12. It is worth noting that the flux reduction in the doped cases with neptunia and americia compared to the reference case (as noted above due to the fission inventories that increase more over time) is larger than that observed with a poison content of 1.5 at.%.

5.2.1. Poisonousness

The infinite multiplication factors at BoL of all cases and the reductions in the initial criticality of the doped cases versus the undoped case (UO_2) are shown in Table 13.

From these values, the following order is found: Eu_2O_3, B_4C, AmO_2, Gd_2O_3, NpO_2, Dy_2O_3, Er_2O_3. Again, the comparison with the order derived from Table 4 is very good overall. While however in the previous comparison AmO_2 and B_4C were inverted, here the inversion is between the cases with NpO_2 and Gd_2O_3. Although inaccurate, this result does not affect the interpretation that can be drawn from it. In fact, the two cases are not distinguishable from each other, as their discrepancy (28 pcm) is totally within the statistical uncertainty of the calculations. Moreover, the corresponding poisonousness values in Table 4 (0.25 vs 0.24), although reversed, are also very close to each other, reflecting the fact that even for the model these two materials have very similar poisonousness.

5.2.2. Burnability

The reactivity swing values at increasing burnup steps for the different cases are given in Table 14. From these values, it can be seen that the order of the cases, from the smallest to the largest, is basically the same regardless of the burnup value. Exceptions are the cases with Er_2O_3 and UO_2 that show an opposite trend as burnup increases. However, these cases are never really distinguishable from each other, since the discrepancies between their reactivity swings are always lower than the statistical uncertainty of the calculations.

In Table 15 the order of the results in terms of reactivity swing reduction obtained with MCNP6.1 is compared with that inferred from the values in Table 7.

Regarding the comparison in Table 15, the following is observed.

- for burnups lower than 47.91 GWd/t_{HM}, excellent agreement is observed except for Eu_2O_3, whose performance at low burnups continues to be strongly underestimated by the model (even if it increases as burnup increases) and for Er_2O_3, which the model slightly overestimates;
- for burnups above 63.89 GWd/t_{HM}, excellent agreement is observed, the order being fully respected.

Differently from the case with 1.5 at.%, it is here observed that the model's predictions on the relative effectiveness of the burnable poisons with respect to the non-doped case (UO_2, reference) are better matching the simulations, as the systematic overestimation of Gd_2O_3 and Dy_2O_3 at low burnups is not found anymore.

6. Discussion

The outcomes of the comparison carried out in the previous paragraph allow us to confirm the ability of the model in predicting the neutronic behavior of a material used up to 10 at.% as a burnable poison, in a broad range of burnups and especially above 60 GWd/t_{HM}. Despite this non-trivial conclusion, to better understand the neutronic reasons behind the effectiveness of the model, its main approximations are analyzed in the following. These have to do with using.

- an approximate spectrum to calculate the cross sections;
- one-group effective cross sections;
- the same flux in the poison and fuel regions even with heterogeneous configurations.

Regarding the first approximation, it can be seen that the spectrum is approximated in a twofold sense.

- it does not account for effects due to the burnable poison itself, being calculated without a detailed configuration in terms of geometry and materials;
- it does not account for effects due to depletion being assumed to be independent of time (according to the constant cross section approximation).

Table 16
Relative difference [%] between simulation and model reaction rates.

Case	Isot.	0 GWd/t_{HM}		159.71 GWd/t_{HM}	
		1.5 at.%	10 at.%	1.5 at.%	10 at.%
(n,f) reaction rates					
$(U,Eu)O_2$	^{235}U	+1.39	+9.10	+70.59	+81.23
$(U,Gd)O_2$	^{235}U	+1.63	+10.59	+71.49	+85.32
$(U,Dy)O_2$	^{235}U	+1.65	+10.77	+71.49	+85.58
$(U,Er)O_2$	^{235}U	+1.72	+11.08	+71.63	+86.35
$(U,Np)O_2$	^{235}U	+0.19	−0.64	+65.48	+47.08
	^{237}Np	−0.79	+7.29	+36.03	+32.61
	^{238}Pu			+48.39	+38.10
	^{239}Pu			+56.43	+42.20
	^{240}Pu			+39.43	+34.30
	^{241}Pu			+65.57	+46.57
$(U,Am)O_2$	^{235}U	+0.59	+1.90	+66.45	+51.93
	^{241}Am	−0.28	+12.73	+36.62	+37.45
	^{242m}Am			+64.01	+50.52
	^{243}Am	−0.34	+12.93	+36.51	+37.60
	^{242}Cm			+45.01	+40.76
	^{243}Cm			+62.86	+49.96
	^{244}Cm			+39.41	+38.16
	^{245}Cm			+64.73	+50.97
	^{246}Cm			+38.67	+38.20
UO_2+B_4C	^{235}U	+0.80	+4.74	+70.48	+78.40
(n,γ) reaction rates					
$(U,Eu)O_2$	^{151}Eu	+0.22	−5.28	+94.17	+82.15
	^{152}Eu			+87.00	+82.61
	^{153}Eu	+0.21	−5.31	+94.39	+82.15
	^{154}Eu			+92.75	+82.82
	^{155}Eu			+102.28	+81.57
	^{156}Eu			+102.23	+80.62
	^{152}Sm			+85.54	+80.75
	^{152}Gd			+82.64	+80.22
	^{153}Gd			+97.16	+82.53
$(U,Gd)O_2$	^{154}Gd	+2.99	+10.35	+92.54	+103.03
	^{155}Gd	+3.31	+10.63	+97.94	+108.97
	^{156}Gd	+2.86	+9.38	+92.97	+100.74
	^{157}Gd	+3.65	+10.30	+103.60	+112.99
	^{158}Gd	+2.75	+7.76	+94.39	+97.03
	^{160}Gd	+2.65	+7.75	+95.60	+99.80
	^{159}Tb			+93.30	+105.59
	^{160}Dy			+89.60	+101.06
	^{161}Dy			+100.69	+111.71
	^{162}Dy			+98.84	+108.50
$(U,Dy)O_2$	^{160}Dy	+2.94	+11.09	+89.68	+102.01
	^{161}Dy	+3.59	+11.46	+100.78	+113.11
	^{162}Dy	+2.82	+8.40	+96.25	+99.63
	^{163}Dy	+3.62	+10.78	+101.96	+112.03
	^{164}Dy	+2.99	+7.45	+100.20	+101.73
$(U,Er)O_2$	^{164}Er	+2.99	+12.14	+88.16	+102.46
	^{165}Ho			+86.19	+111.45
	^{166}Er	+2.66	+10.56	+88.94	+100.04
	^{167}Er	+3.40	+12.33	+95.87	+109.45
	^{168}Er	+2.69	+9.67	+90.12	+95.69
	^{169}Er			+89.83	+116.04
	^{170}Er	+2.73	+9.58	+95.04	+102.75
	^{169}Tm			+87.61	+113.08
	^{170}Tm			+88.46	+114.27
$(U,Np)O_2$	^{237}Np	+0.62	−3.98	+80.17	+52.70
	^{238}Pu			+79.11	+53.33
	^{239}Pu			+91.70	+60.65
	^{240}Pu			+79.65	+54.31
	^{241}Pu			+78.48	+53.85
$(U,Am)O_2$	^{241}Am	+0.75	−1.12	+75.98	+56.91
	^{242m}Am			+75.19	+56.61
	^{243}Am	+0.69	−1.89	+77.97	+58.06
	^{242}Cm			+78.41	+58.26
	^{243}Cm			+74.24	+56.03
	^{244}Cm			+81.68	+59.82
	^{245}Cm			+73.81	+55.80
	^{246}Cm			+82.99	+60.63
(n,α) reaction rate					
UO_2+B_4C	^{10}B	+0.12	+6.77	+93.18	+114.40

Table 17
Difference [%] between the ratios of the capture and fission reaction rates in the simulation and model cases.

Case	0 GWd/t_{HM}	159.71 GWd/t_{HM}		
	1.5 at.%	10 at.%	1.5 at.%	10 at.%
$(U,Eu)O_2$	98.84	86.81	112.88	100.53
$(U,Gd)O_2$	101.58	99.61	114.72	111.81
$(U,Dy)O_2$	101.69	99.96	115.68	112.48
$(U,Er)O_2$	101.33	100.65	110.43	111.84
$(U,Np)O_2$	100.61	95.20	114.87	108.39
$(U,Am)O_2$	100.37	93.95	110.76	106.08
UO_2+B_4C	99.09	101.94	113.32	120.17

Both approximations arise from the model's need to calculate cross sections as simply as possible. Of course, each of them involves an error in the calculation of reaction rates. To get an idea of their impact, the reaction rates over the entire energy range obtained from the simulations have been compared with those obtained from the model. This was done for the initial isotopes as a function of burnup. The relative difference values for burnups of 0 and 159.71 GWd/t_{HM} are shown in Table 16. As can be seen, except for some cases (such as fission reaction rates of ^{235}U in $(U,Np)O_2$ and radiative capture reaction rates of ^{151}Eu and ^{153}Eu in $(U,Eu)O_2$ and of ^{241}Am and ^{243}Am in $(U,Am)O_2$), the higher the poison content, the greater the error. In fact, by increasing the poison content up to 10 at.%, the values increase up to 15 %. But much more relevant in terms of the distance between simulation and model is, as expected, the increase in burnup. In this case, the relative differences between reaction rates increase from a few percent to about 100 %.

Although these differences are often relevant, the effectiveness of the model does not seem to be greatly affected. Indeed, even in the absence of an error propagation analysis, it is possible to affirm that the errors in reaction rates do not cause a discrepancy between nominal values of the quantities of interest (namely, poisonousness and burnability) such that the model results be compromised (as confirmed by the very good agreement between simulations and model).

To better understand the basis of this very good agreement, we first calculated the ratio of capture reaction rates (any absorption except fission) to fission reaction rates for both simulation and model cases and then made the ratio between the two ratios, as can be seen in Eq. (13):

$$\frac{\left[\frac{\sum_i (RR_c)_i}{\sum_j (RR_f)_j}\right]_{simul.}}{\left[\frac{\sum_i (RR_c)_i}{\sum_j (RR_f)_j}\right]_{model}} \tag{13}$$

where i and j refer, for each case, to the main isotopes involved in capture and fission, respectively.

As can be noted from the values in Table 17 (calculated including, for each burnup step, the isotopes reported in Table 16), the approximations on the spectrum have a low impact on the ratio of captures to fissions in the model cases compared to the simulated cases. This is especially true at a burnup of 0 GWd/t_{HM} regardless of the poison content (where the maximum difference is in the case with europia at 10 at.%). But even at very high burnup, the discrepancy never exceeds 20 %. The physical reason behind these results is probably due to the fact that the trends of cross sections as a function of energy are largely similar for the isotopes considered.

The use of one-energy-group cross sections is another strong approximation of the model that again stems from the need to make the model as simple as possible. Although the model results were found to be in good agreement with the simulations, it is worth asking why this approximation works and whether a justified benefit would result by using cross sections at more energy groups.

As a general rule, regardless of the number of energy groups, the trend of the cross sections of the isotopes to be compared must be taken

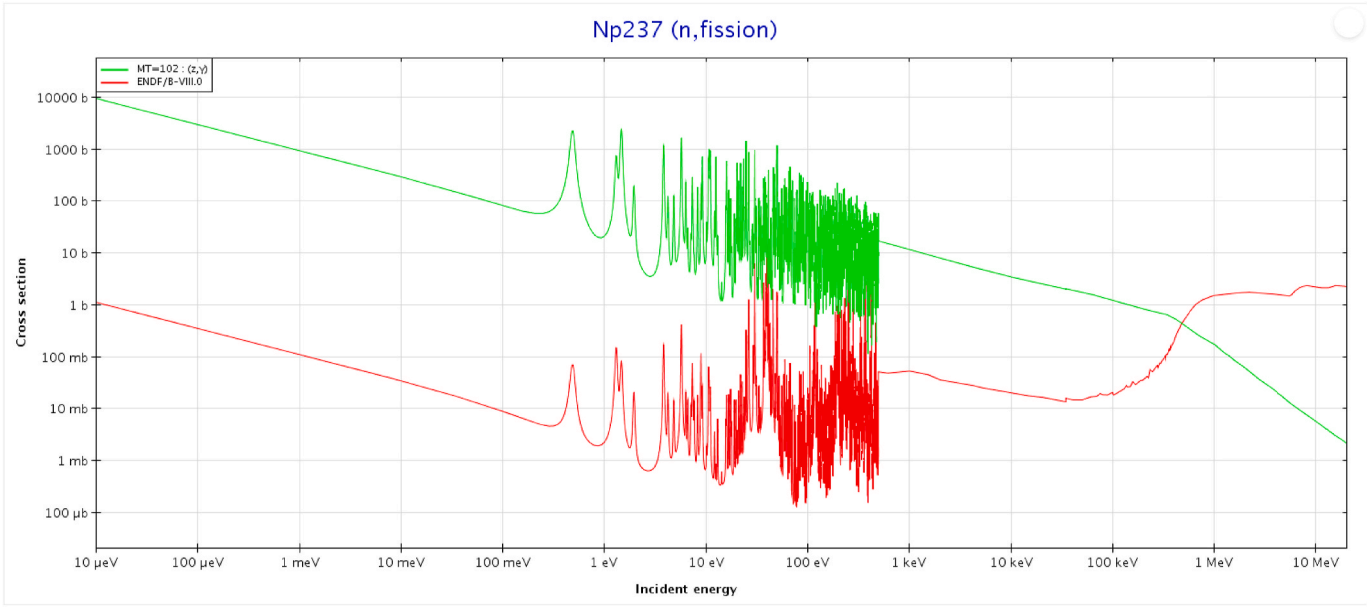

Fig. 5. Fission (red line) and capture (green line) cross sections of ^{237}Np.[11] (For interpretation of the references to colour in this figure legend, the reader is referred to the Web version of this article.)

Table 18
Poisonousness values with one and two-groups cross sections.

Case	One-group xs	Two-groups xs	
		<1.11E-01 MeV	>1.11E-01 MeV
Eu_2O_3	−9.0	−28.6	−2.4
Gd_2O_3	−2.4	−7.8	−0.6
Dy_2O_3	−2.3	−7.6	−0.6
Er_2O_3	−2.0	−6.3	−0.6
NpO_2	−2.5	−14.4	+1.5
AmO_2	−3.5	−15.9	+0.6
B_4C	−3.9	−11.6	−1.3

Table 19
Two-groups effective cross sections for the initial isotopes.

Isotope	Energy range [MeV]	
	<1.11E-01	>1.11E-01
$\nu\sigma_f$		
^{235}U	5.57 (=2.42·2.30)	3.16 (=2.51·1.26)
^{237}Np	0.05 (=2.64·0.02)	1.62 (=2.85·0.57)
^{238}U	0.00 (=2.45·0.00)	0.19 (=2.72·0.07)
^{241}Am	0.06 (=3.09·0.02)	1.45 (=3.37·0.43)
^{243}Am	0.03 (=3.28·0.01)	1.10 (=3.54·0.31)
σ_γ		
^{151}Eu	4.54	0.83
^{153}Eu	3.33	0.53
^{154}Gd	1.15	0.31
^{155}Gd	3.19	0.51
^{156}Gd	0.73	0.18
^{157}Gd	1.78	0.24
^{158}Gd	0.36	0.08
^{160}Gd	0.20	0.03
^{160}Dy	0.98	0.27
^{161}Dy	2.45	0.31
^{162}Dy	0.55	0.11
^{163}Dy	1.36	0.20
^{164}Dy	0.27	0.04
^{164}Er	2.27	0.64
^{166}Er	0.79	0.15
^{167}Er	1.87	0.32
^{168}Er	0.33	0.07
^{170}Er	0.26	0.04
^{235}U	0.79	0.21
^{237}Np	2.38	0.54
^{238}U	0.42	0.11
^{241}Am	2.66	0.80
^{243}Am	2.60	0.55
(n,α) cross section		
^{10}B	3.98	0.94

into account. In fact, it is necessary that, in each energy group, the total net contribution to the neutron balance – i.e. $(\nu\sigma_f - \sigma_a)$ – is consistent for all isotopes.

In the present work, for example, such consistency is not verified at energies above about 0.1 MeV. In fact, the isotopes ^{237}Np, ^{241}Am and ^{243}Am have opposite total net contributions to the neutron balance compared to the other isotopes, due to the opposite trends of fission and radiative capture cross sections at those energies (for ^{237}Np these two cross sections as a function of energy are shown in Fig. 5).

To assess the impact that the use of the two-groups cross sections would have on the present study, the model results in terms of poisonousness have been recalculated. In this regard, the threshold between fast and non-fast energies was assumed to be 1.11E-01 MeV (a value very close to the reference one but part of the energy group structure used for simulations) and the flux values corresponding to the two energy ranges were chosen equal to 8.0112E+13 and 1.1518E+14 cm^{-2} s^{-1}, respectively.

As can be seen from the values in Table 18, the final orders obtained with two-groups cross sections are basically in agreement with the previous one except for the cases of NpO_2 and AmO_2 in the fast group. In fact, for energies above 1.11E-01 MeV their values become positive.

This is confirmed by the analysis of the two-groups effective cross sections in Table 19 where it can be seen that, for ^{237}Np, ^{241}Am and ^{243}Am, $\nu\sigma_f$ is greater than σ_a at energies above 1.11E-01 MeV, making the term $(\nu\sigma_f - \sigma_a)$ and thus the corresponding poisonousness value positive.

In case the consistency of the total net contribution to the neutron balance in each energy group is verified for all isotopes to be compared, the choice of the type of cross sections to be used should be made according to the type of spectrum. In this regard, it seems reasonable to use one-group cross sections with fast spectra, while the use of two-groups cross sections should be carefully considered with solutions involving spectra with a relevant epithermal fraction. The latter is, for instance, the case described in [Guo, 2020], where, in a sodium fast reactor, Zr_5H_8

Table 20
Residual reactivity penalty [pcm] as a function of burnup [GWd/t_{HM}] for both poison contents.

Case	15.97	31.94	47.91	63.89	95.83	159.71
1.5 at.% poison content						
$(U,Eu)O_2$	3658	3755	3779	3786	3766	3703
$(U,Gd)O_2$	1177	1209	1244	1285	1354	1494
$(U,Dy)O_2$	1150	1193	1221	1259	1324	1463
$(U,Er)O_2$	1021	1046	1086	1134	1206	1379
$(U,Np)O_2$	1232	1074	940	774	421	−265
$(U,Am)O_2$	1528	1375	1206	1020	648	−28
UO_2+B_4C	1576	1499	1429	1374	1198	937
10 at.% poison content						
$(U,Eu)O_2$	23475	24112	24568	24913	25393	25868
$(U,Gd)O_2$	8397	8664	8912	9169	9694	10733
$(U,Dy)O_2$	8205	8473	8729	8999	9473	10414
$(U,Er)O_2$	7245	7544	7846	8132	8758	9904
$(U,Np)O_2$	7207	6251	5294	4291	2254	−1535
$(U,Am)O_2$	9137	7991	6869	5759	3621	−164
UO_2+B_4C	11309	10889	10425	9907	8912	6862

Table 21
Predictivity of the model with respect to residual reactivity penalty as a function of burnup [GWd/t_{HM}].

Case	15.97	31.94	47.91	63.89	95.83	159.71
Simulations (MCNP) with 1.5 at.% poison content						
Best	Er_2O_3	Er_2O_3	NpO_2	NpO_2	NpO_2	NpO_2
2	Dy_2O_3	NpO_2	Er_2O_3	AmO_2	AmO_2	AmO_2
3	Gd_2O_3	Dy_2O_3	AmO_2	Er_2O_3	B_4C	B_4C
4	NpO_2	Gd_2O_3	Dy_2O_3	Dy_2O_3	Er_2O_3	Er_2O_3
5	AmO_2	AmO_2	Gd_2O_3	Gd_2O_3	Dy_2O_3	Dy_2O_3
6	B_4C	B_4C	B_4C	B_4C	Gd_2O_3	Gd_2O_3
Worst	Eu_2O_3	Eu_2O_3	Eu_2O_3	Eu_2O_3	Eu_2O_3	Eu_2O_3
Simulations (MCNP) with 10 at.% poison content						
Best	NpO_2	NpO_2	NpO_2	NpO_2	NpO_2	NpO_2
2	Er_2O_3	Er_2O_3	AmO_2	AmO_2	AmO_2	AmO_2
3	Dy_2O_3	AmO_2	Er_2O_3	Er_2O_3	B_4C	B_4C
4	Gd_2O_3	Dy_2O_3	Dy_2O_3	Dy_2O_3	Er_2O_3	Er_2O_3
5	AmO_2	Gd_2O_3	Gd_2O_3	Gd_2O_3	Dy_2O_3	Dy_2O_3
6	B_4C	B_4C	B_4C	B_4C	Gd_2O_3	Gd_2O_3
Worst	Eu_2O_3	Eu_2O_3	Eu_2O_3	Eu_2O_3	Eu_2O_3	Eu_2O_3
Model						
Best	Er_2O_3	Er_2O_3	NpO_2	NpO_2	NpO_2	NpO_2
2	NpO_2	NpO_2	Er_2O_3	Er_2O_3	Er_2O_3	AmO_2
3	Dy_2O_3	Dy_2O_3	Dy_2O_3	AmO_2	AmO_2	Er_2O_3
4	Gd_2O_3	Gd_2O_3	Gd_2O_3	Dy_2O_3	Dy_2O_3	Dy_2O_3
5	AmO_2	AmO_2	AmO_2	Gd_2O_3	Gd_2O_3	Gd_2O_3
6	B_4C	B_4C	B_4C	B_4C	B_4C	B_4C
Worst	Eu_2O_3	Eu_2O_3	Eu_2O_3	Eu_2O_3	Eu_2O_3	Eu_2O_3

has been coupled with B_4C in dedicated control assemblies to take advantage of the very high capture cross section of ^{10}B in the thermal domain.

The third approximation we wanted to test concerns the use of the same flux in the poison and fuel regions in presence of heterogeneous configurations when poison and fuel are placed in different rods. This approximation is used in the calculation of both quantities. This is a forced approximation, due to the aim of applying the model before defining an actual configuration from which to possibly estimate a ratio between fluxes. However, besides being theoretically justified for fast spectra, this approximation has also been confirmed by simulation results. In fact, the ratio of the average flux in B_4C region to that in the UO_2 region was found to be never lower than 97.6 % and reaches 99.7 % at a burnup of 159.71 GWd/t_{HM} for both poison contents.

A last point that deserves to be addressed concerns the possibility of extending the prediction ability of the model to the residual reactivity penalty (as introduced in section 2.3). The equation derived from the ratio of e_{POIS} to $(1 + e_{BURN})$, although it is physically consistent with the attributes of poisonousness and burnability, has not proven to be effective. Instead, the formula that best fits the values calculated from the simulations, thus providing information on the behavior of a material in terms of its residual reactivity penalty, was found to be the following:

$$e_{RRP} = \left| \frac{e_{POIS}}{(1 + e_{BURN})^2} \right| \tag{14}$$

Note that, when burnup is zero (and thus $e_{BURN} = 0$), the equation gives the absolute value of the poisonousness.

The predictivity of Eq. (14) was evaluated against the results obtained from simulations. In this regard, the values of residual reactivity penalty as a function of burnup calculated by means of MCNP6 are given in Table 20 for both poison contents.

The comparison, as a function of burnup, between the order of the results of the simulations in Table 20 and the order of the results obtained with Eq. (14) is shown in Table 21. Although there are some differences, including in particular an underestimation of the reactivity penalty of B_4C and AmO_2 cases, respectively, at very high burnup (that is at 95.83 and 159.71 GWd/t_{HM}) and between 31.94 and 95.83 GWd/t_{HM}, the result of the comparison is overall acceptable. This is even more so when one considers that the order of the results from simulations is not preserved as the poison content changes.

7. Conclusions

The model presented in this paper addresses the need to estimate the neutronic performance of materials to be used as burnable poisons in small modular liquid-metal-cooled fast reactors. In fact, although burnable poisons are a viable (and sometime forced) route to extend the core lifetime or to reduce the effects of possible accidents involving CRs in such reactors, to date very few materials are known that may be used as burnable poisons in fast spectrum.

The model has been designed to evaluate a material according to its effectiveness in controlling the positive reactivity in a given time. For this purpose, performance due to its poisonousness, defined as the ability to provide enough initial negative reactivity to compensate for the excess reactivity of the fresh fuel, was evaluated separately from performance due to its burnability, which takes into account the ability to balance the reactivity change due to fuel depletion. The values calculated by the model's equations for these attributes (poisonousness and burnability) can be used in a comparison of materials to obtain an estimate of their neutronic behaviour.

The model was first tested and then assessed. In the test phase, seven candidates such as Eu_2O_3, Gd_2O_3, Dy_2O_3, Er_2O_3, NpO_2, AmO_2 and B_4C were chosen and, for each of them, values of poisonousness and burnability were calculated. The material order derived from the model results were then compared with the one obtained with extensive calculations with MCNP6.1 for a lead-cooled fast reactor fuel assembly with UO_2 enriched in ^{235}U at 19.75 wt%, in which the various candidates were, one at a time, added. In this regard, the first six candidates were mixed homogeneously with the fuel while B_4C was placed in dedicated pins. The assessment was performed with two poison contents, namely 1.5 and 10 at.%, to assess how much this parameter might affect the model response. Despite some minor differences, the comparison largely confirmed the prediction capability of the model in reproducing the ranking of the candidates in the burnup range of 16–160 GWd/t_{HM} with both poison contents.

Finally, from the combination of poisonousness and burnability, a formula was derived that evaluates the behavior of materials in terms of their residual reactivity penalty.

Albeit promising, this work suggests the possibility for further extensions, two of which are noteworthy. First, a broader assessment of the model, which should be extended to other fast reactors (for example,

[1] See https://www.oecd-nea.org/janisweb/.

SFRs). Second, the application of the model to other candidates to find new materials that exhibit neutronic behaviors consistent with those of a burnable poison.

CRediT authorship contribution statement

Roberto Pergreffi: Writing – review & editing, Writing – original draft, Software, Resources, Methodology, Investigation, Data curation, Conceptualization. **Francesco Lodi:** Writing – review & editing, Supervision, Methodology, Conceptualization. **Giacomo Grasso:** Writing – review & editing, Supervision. **Alessia Di Francesco:** Writing – original draft, Software, Data curation.

Declaration of competing interest

The authors declare that they have no known competing financial interests or personal relationships that could have appeared to influence the work reported in this paper.

Acknowledgments

The computing resources and the related technical support used for this work have been provided by CRESCO/ENEAGRID High Performance Computing infrastructure and its staff. CRESCO/ENEAGRID High Performance Computing infrastructure is funded by ENEA, the Italian National Agency for New Technologies, Energy and Sustainable Economic Development and by Italian and European research programmes, see http://www.cresco.enea.it/english for information.

APPENDIX A

An example of the burnability calculation is given below for neptunium assumed as 100 % ^{237}Np. Starting from the reactions of the corresponding simplified chain in Fig. 1 and including the transmutations due to fission reactions of the fissile isotopes, Eq. (15) is written:

$$\begin{aligned} e_{BURN} = {} & (x_{48} - x_{37})^{*}A_{d_{48}} + (x_{49} - x_{48})^{*}A_{d_{49}} + \\ & (x_{40} - x_{49})^{*}A_{d_{40}} + (x_{41} - x_{40})^{*}A_{d_{41}} + \\ & (-x_{37})^{*}A_{p_{fiss_{37}}} + (-x_{48})^{*}A_{p_{fiss_{48}}} + \\ & (-x_{49})^{*}A_{p_{fiss_{49}}} + (-x_{40})^{*}A_{p_{fiss_{40}}} + \\ & (-x_{41})^{*}A_{p_{fiss_{41}}} \end{aligned} \quad (15)$$

To identify the various isotopes, the notation involving a double subscript *ij* was used, where *i* is the last digit of the atomic number and *j* is the last digit of the mass number. The contributions to burnability due to radiative capture and fission reactions are expressed by the first four and last five terms in the right-hand side of the equation, respectively. For each term, it is necessary to calculate the atom fraction of the corresponding isotope over a given time interval. For example, to calculate the atom fraction of ^{238}Pu i.e., $A_{d_{48}}$, the evolution equation of its parent isotope ^{237}Np must be known (actually, absorbing a neutron ^{237}Np transmutes into ^{238}Np which, in turn, transforms into ^{238}Pu with a beta minus decay, but since ^{238}Np has a half-life of 2.117 days, we can consider ^{238}Pu as produced directly upon capture by ^{237}Np). Since we are only interested in the transmutation of the quantity added as burnable poison, this equation must contain the removal term (due to any kind of absorption) but not the production term:

$$\frac{dA_{p_{37}}}{dt} = -A_{p_{37}}(t)\sigma_a\phi \quad (16)$$

Upon integration between an initial time when the atom fraction of ^{237}Np is $A_{p_{37}}(0)$, and a time t later, the solution becomes:

$$A_{p_{37}}(t) = A_{p_{37}}(0)e^{-\sigma_a^{37}\phi t} \quad (17)$$

Then, by integrating the reaction rate of radiative capture over time, the equation of $A_{d_{48}}$ as a function of time is obtained:

$$\begin{aligned} A_{d_{48}}(t) = {} & \int A_{p_{37}}(t)\sigma_\gamma^{37}\phi dt = \\ & A_{p_{37}}(0)\sigma_\gamma^{37}\phi \int e^{-\sigma_a^{37}\phi t}dt = \\ & \frac{A_{p_{37}}(0)\sigma_\gamma^{37}}{\sigma_a^{37}}\left(1 - e^{-\sigma_a^{37}\phi t}\right) \end{aligned} \quad (18)$$

Knowing $A_{p_{37}}(t)$, the atom fraction of ^{237}Np undergoing fission reactions $A_{p_{fiss_{37}}}$ is calculated as follows:

$$\begin{aligned} A_{p_{fiss_{37}}}(t) = {} & \int A_{p_{37}}(t)\sigma_f^{37}\phi dt = \\ & A_{p_{37}}(0)\sigma_f^{37}\phi \int e^{-\sigma_a^{37}\phi t}dt = \\ & \frac{A_{p_{37}}(0)\sigma_f^{37}}{\sigma_a^{37}}\left(1 - e^{-\sigma_a^{37}\phi t}\right) \end{aligned} \quad (19)$$

Once the atom fractions of all daughter isotopes A_d and all parent fissile isotopes undergoing fission reactions $A_{p_{fiss}}$ have been calculated over a given time interval, the burnability of ^{237}Np in that time can be determined by substituting these values in Eq. (15). As an example, the values of these variables over a 50-year interval are summarized for each isotope in Table 22.

Table 22
Values of the variables for calculating the burnability of ^{237}Np.

Isotope	Isotope notation	$\nu\sigma_f - \sigma_a = x$ [barn]	A_d [%]	$A_{P_{fiss}}$ [%]
^{237}Np	37	−0.67	–	0.043
^{238}Pu	48	1.61	0.164	0.044
^{239}Pu	49	2.90	0.021	0.006
^{240}Pu	40	0.37	0.001	0.000
^{241}Pu	41	4.04	0.000	0.000

APPENDIX B

The geometric and material data and the calculation settings used to obtain the cross sections for the model are detailed below. In this calculation the following materials are used.

- as fuel, UO_2 enriched in ^{235}U to 19.75 wt% (the composition of the uranium vector is reported in Table 23);
- as gas in the gap between fuel and cladding, helium;
- as cladding, the low-swelling austenitic stainless steel AIM1 of class “15-15Ti” [Angiolini, 2017];
- as coolant, a commercial nuclear-grade lead that meets the so called “C1” Russian standard [Ivanov, 2003].

Table 23
Isotopic composition [wt.%] of uranium vector.

Isotope	Value
^{234}U	0.1868
^{235}U	19.7500
^{238}U	80.0632

The corresponding mass densities at room temperature are given in Table 24. It is worth noting that the density of lead is a fictitious value (representing the density that the lead would have if it were liquid at 20 °C) usually used to simplify the calculation of the actual density in operating conditions [NEA, 2015].

Table 24
Mass densities [g/cm^3] at room temperature.

Material	Value
UO_2	10.322
Helium	0.001
Stainless Steel	7.972
Lead	11.066

The geometric dimensions of the hexagonal fuel cell at room temperature are given in Table 25. No thermal expansion was done. Radial and axial reflective boundary conditions were assumed.

Table 25
Geometric data of the fuel cell at room temperature.

Parameter	Value [cm]
Fuel radius	0.450
Inner clad radius	0.465
Outer clad radius	0.525
Lattice pitch	1.300
Active height	1.000

The cross-sectional view of the fuel cell is shown in Fig. 6.

The operating temperatures for Doppler broadening of the cross-sections are 900 K for the fuel and 600 K for the other materials according to the set available in ENDF/B-VIII.0.

To minimize statistical variations, 110 k-eigenvalue source iteration cycles, of which the first 10 skipped, with 1.0E+05 histories per cycle are used. This choice corresponds to a relative error at one standard deviation of the reaction rates by MCNP6 never exceeding 0.05 %.

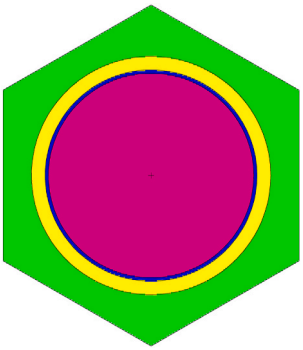

Fig. 6. Cross-sectional view of the fuel cell used as simulation domain.

APPENDIX C

The main modelling aspects of the MCNP simulations with poison contents of 1.5 and 10 at.% are discussed here.
In these simulations, the following materials are used.

- as fuel in the reference FA and in the heterogeneously doped FA, UO_2 enriched in ^{235}U at 19.75 wt%;
- as material of the pellet in the homogeneously doped FAs, a mixture of UO_2 (enriched in ^{235}U at 19.75 wt%) and poison oxide (i.e., Eu_2O_3, Gd_2O_3, Dy_2O_3, Er_2O_3, NpO_2, AmO_2);
- as absorber in the heterogeneously doped FA, B_4C with boron enriched in ^{10}B to 90 at.%;
- as gas, cladding and coolant, the same materials used in the test phase;
- as wrapper, the same steel used for the cladding.

The atom densities of the materials in the homogeneously doped FAs were calculated by mixing the atom densities of the two initial oxides according to the following formula:

$$\rho_{mixture} = \frac{1}{\frac{y_1/100}{\rho_1} + \frac{y_2/100}{\rho_2}} \tag{20}$$

where y and ρ are, respectively, the percentage content and atom density in [at/barn/cm] of the oxides (i.e., uranium oxide and poison oxide) of which the mixture is composed.

The atom densities at room temperature of each case are shown in Table 26.

Table 26
Atom densities [atoms/barn/cm] at room temperature.

Case	1.5 at.%.	10 at.%.
UO_2	0.0728517	
$(U.Eu)O_2$	0.0726908	0.0717924
$(U.Gd)O_2$	0.0725897	0.0711405
$(U.Dy)O_2$	0.0726805	0.0717256
$(U.Er)O_2$	0.0727741	0.0723375
$(U.Np)O_2$	0.0728764	0.0730167
$(U.Am)O_2$	0.0729124	0.0732587
B_4C	0.1374587	

Table 27
Geometric data [cm] of the FAs at room temperature.

Parameters	1.5 at.%	10 at.%
Hollow radius	0.1000	
UO_2 pellet radius	0.4500	
$(U,Eu)O_2$ pellet radius	0.4505	0.4531
$(U,Gd)O_2$ pellet radius	0.4508	0.4551
$(U,Dy)O_2$ pellet radius	0.4505	0.4533
$(U,Er)O_2$ pellet radius	0.4502	0.4515
$(U,Np)O_2$ pellet radius	0.4499	0.4495
$(U,Am)O_2$ pellet radius	0.4498	0.4488
UO_2 pellet radius in heterog. case	0.4486	0.4393
B_4C pellet radius in heterog. case	0.4352	0.4488

(*continued on next page*)

Table 27 (*continued*)

Parameters	1.5 at.%	10 at.%
Cladding inner radius	0.4650	
Cladding outer radius	0.5250	
Pins lattice pitch	1.3000	
Wrapper inner flat-to-flat	28.400	
Wrapper outer flat-to-flat	28.900	
FA lattice pitch (with lead bypass)	29.100	
Active height	100.000	

The geometry corresponds to a hexagonal FA with 13 rings and 469 rod positions, limited axially to only the active height. As typical in FRs, a cylindrical hollow coaxial with the pellet itself (whether UO_2 or $(U,BP)O_2$) was considered. The same cylindrical hollow was also applied to the B_4C pellet to avoid a too small radius compared with that of the cladding. The geometric data at room temperature are collected in Table 27. It is worth noting that the difference in the pellet radii of the different doped cases is due to the difference in the atom densities of the different oxides.

The number of absorber rods in the B_4C-doped FAs depends on the poison content. Specifically, by increasing the poison content from 1.5 to 10 at.%, the absorbent rods increase from 4 to 25. The cross-sectional views of these assemblies are shown in Figs. 7 and 8, respectively. In both configurations, the positioning of the absorber rods was chosen so as to minimize the shadowing effect as much as possible.

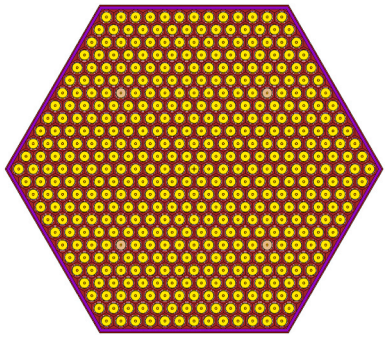

Fig. 7. Cross-sectional view of the B_4C-doped FA with 1.5 at.% poison content.

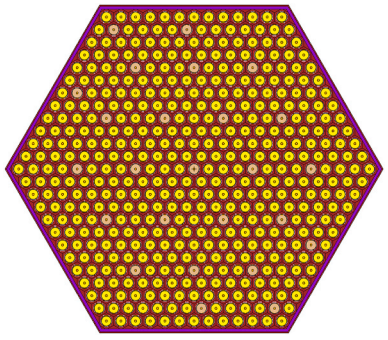

Fig. 8. Cross-sectional view of the B_4C-doped FA with 10 at.% poison content.

Unlike the test phase, the geometry was expanded. Operating temperatures and corresponding instantaneous coefficients of linear thermal expansion (α_L) for fuel (whether UO_2 or $(U,BP)O_2$), absorber (B_4C), cladding and FA wrapper are shown in Table 28. Although the thermal expansion of the uranium-BP oxides is different in the various cases, the same value as that used for the UO_2 was assumed as a first approximation. Moreover, the total volumetric expansion was assumed to be equally distributed among the three axes, hence $\alpha_V \cong 3\alpha_L$.

Table 28
Operating temperatures and coefficients of linear thermal expansion of fuel, cladding and FA wrapper.

Material	Temp. [K]	$10^6 \langle\alpha_L\rangle$ [K^{-1}]	$10^3 \varepsilon$ [-]	Source
Fuel	873.15	9.969	5.782	[Martin, 1988]
B_4C	673.15	3.868	1.470	[Thévenot, 1990]
Cladding	673.15	17.82	6.773	[Sobolev, 2011]
Wrapper	668.15	17.82	6.682	[Sobolev, 2011]

The mass density of the coolant at 668.15 K was computed according to the following equation [NEA, 2015]:

$$\rho = 11441 - 1.2795*T \tag{21}$$

where, for temperature T in [K], the density is in [kg/m^3].

Radial and axial reflection boundary conditions were assumed.

The temperatures for Doppler broadening of the cross-sections are the same as those used in the test phase as well as the input parameters of the criticality source (which still determine a relative error at one standard deviation of the reaction rates of less than 0.05 %).

Depletion calculations were performed to attain, in all doped cases, the same burnup steps as those of the reference case (UO_2). The burnup steps are as follows (in GWd/t_{HM}): 1.05, 3.19, 15.97, 31.94, 47.91, 63.89, 95.83, 159.71.

Since the doped cases have the same nominal thermal power (2.375 MW_{th}) but different heavy metal inventories (due to both the different mixtures and the different poison content), the times needed to achieve the same burnups as in the undoped reference case are forced to vary, as can be seen in Table 29. It should be noted that in the cases with neptunia and americia, these values were obtained by including the initial masses of the minor actinides among those of the heavy metals.

Table 29
Time [years] to reach the same burnup steps [GWd/t_{HM}].

Case	15.97	31.94	47.91	63.89	95.83	159.71
UO_2 (ref.)	5.00	10.00	15.00	20.00	30.00	50.00
With 1.5 at.% poison content						
$(U,Eu)O_2$	4.93	9.86	14.79	19.72	29.58	49.30
$(U,Gd)O_2$	4.93	9.86	14.79	19.72	29.58	49.31
$(U,Dy)O_2$	4.93	9.86	14.79	19.72	29.58	49.29
$(U,Er)O_2$	4.93	9.86	14.78	19.71	29.57	49.28
$(U,Np)O_2$	5.00	10.00	15.00	20.00	30.00	50.00
$(U,Am)O_2$	5.00	10.00	15.00	20.01	30.01	50.01
UO_2+B_4C	4.92	9.85	14.77	19.70	29.55	49.25
With 10 at.% poison content						
$(U,Eu)O_2$	4.53	9.06	13.58	18.11	27.17	45.28
$(U,Gd)O_2$	4.53	9.06	13.60	18.13	27.19	45.32
$(U,Dy)O_2$	4.52	9.05	13.57	18.10	27.14	45.24
$(U,Er)O_2$	4.52	9.03	13.55	18.06	27.09	45.16
$(U,Np)O_2$	5.00	10.00	15.00	20.00	30.00	49.99
$(U,Am)O_2$	5.01	10.02	15.03	20.03	30.05	50.09
UO_2+B_4C	4.50	9.00	13.50	18.00	27.00	45.00

Data availability

Data will be made available on request.

References

Angiolini, M., Pilloni, L., 2017. Specifica Di Fornitura per Una Colata Sperimentale Di Acciaio Austenitico Stabilizzato Al Titanio. ENEA. Technical Report SM-T-S-242.

Asou, M., Porta, J., 1997. Prospects for poisoning reactor cores of the future. Nucl. Eng. Des. 168.

Brown, D.A., et al., 2018. ENDF/B-VIII.0: the 8th major release of the nuclear reaction data library with CIELO-project cross sections, new standards and thermal scattering data. Nucl. Data Sheets 148, 1–142. https://doi.org/10.1016/j.nds.2018.02.001.

Cinotti, L., et al., 2010. Lead-cooled fast reactor (LFR) design: safety, neutronics, thermal, hydraulics, structural mechanics, fuel, core, and plant design. In: Cacuci, Dan Gabriel (Ed.), Handbook of Nuclear Engineering, vol. 4. Springer.

Conlin, J.L., et al., 2018. Release of ENDF/B-VIII.0-based ACE Data Files, Internal Report LA-UR-18-24034. LANL, Los Alamos.

Coursey, J.S., Schwab, D.J., Tsai, J.J., Dragoset, R.A., 2015. Atomic Weights and Isotopic Compositions. National Institute of Standards and Technology, Gaithersburg, MD, version 4.1. http://physics.nist.gov/Comp [2023, 09, 04].

Duderstadt, J., Hamilton, L., 1976. Nuclear Reactor Analysis. John Wiley & Sons, New York.

NUCLEAR ENERGY AGENCY, 2015. Handbook on lead-bismuth eutectic alloy and lead properties, materials compatibility. Thermal-Hydraulics and Technologies, Report NEA-7268. OECD, Paris.

Evans, J.A., DeHart, M.D., Weaver, K.D., Keiser Jr., D.D., 2021. Burnable absorbers in nuclear reactors – a review. Nucl. Eng. Des.

Goorley, J.T., et al., 2013. Initial MCNP6 Release Overview – MCNP6 Version 1.0, Internal Report LA-UR-13-22934. LANL, Los Alamos.

Guo, H., Kooyman, T., Sciora, P., Buiron, L., 2019. Application of minor actinides as burnable poisons in sodium fast reactors. Nucl. Technol.

Guo, H., Buiron, L., Sciora, P., Kooyman, T., 2020. Optimization of reactivity control in a small modular sodium-cooled fast reactor. Nucl. Eng. Technol.

Iannone, F., et al., 2019. CRESCO ENEA HPC clusters: a working example of a multifabric GPFS spectrum scale layout. In: 2019 International Conference on High Performance Computing & Simulation HPCS 2019. Proc. Int. Conf., Dublin.

Ivanov, K.D., et al., 2003. Impurities in lead and lead-bismuth coolants, *fast neutrons reactors Conference*. Obninsk, Russian Federation (in Russian).

Lamarsh, J.R., Baratta, A.J., 2001. Introduction to Nuclear Engineering. Prentice Hall, Upper Saddle River, New Jersey.

Liu, B., Han, J., Liu, F., Sheng, J., Li, Z., 2020. Minor actinide transmutation in the lead-cooled fast reactors. Prog. Nucl. Energy.

Lynn, J.E., Patrick, B.H., Sowerby, M.G., Bowey, E.M., 1980. Evaluation of differential nuclear data for americium isotopes. Part I: ^{241}Am. Prog. Nucl. Energy 5, 255–282.

Martin, D.G., 1988. The thermal expansion of solid UO_2 and (U,Pu) mixed oxides – a review and recommendations. J. Nucl. Mater. 152, 94–101.

Pilate, S., Wiese, H.W., 1988. Reduction of Burnup Reactivity Loss in Large LMFBR Cores by Using Neptunium 237, Jahrestagung Kerntechnik, Travemünde.

Reuss, P., 2008. Neutron physics. EPD Sciences.

Sobolev, V., 2011. Preliminary Recommendations for Thermal and Mechanical Properties of Unirradiated Stainless Steel 15-15Ti. Technical Report I-198, SCK•CEN.

Stacey, W.M., 2001. Nuclear Reactor Physics. John Wiley & Sons, Inc., New York.

Thévenot, F., 1990. Boron Carbide – a comprehensive review. J. Eur. Ceram. Soc. 6, 205–225.